

Delineating the structural controls on iron oxide-Cu-Au deposit genesis through implicit modeling: A case study from the E1 Group, Cloncurry District, Australia

George Case^{1*}, Thomas Blenkinsop^{1,2}, Zhaoshan Chang¹, Jan Marten Huizenga^{1,3}, Richard Lilly⁴ & John McLellan^{1,5}

¹ *Economic Geology Research Centre (EGRU), James Cook University, Townsville, Queensland, 4810, Australia; *Correspondence (george.case@my.jcu.edu.au)*

² *School of Earth and Ocean Sciences, Cardiff University, Cardiff, Wales CF10 3XQ, United Kingdom*

³ *Department of Geology, University of Johannesburg, Auckland Park, Johannesburg, 2006, South Africa*

⁴ *Department of Earth Sciences, University of Adelaide, Adelaide, South Australia, 5005, Australia*

⁵ *Geological Modelling for Exploration (GMEX), PO Box 695, Deeragun, Queensland, 4818, Australia*

Abstract: Iron oxide-Cu-Au (IOCG) deposits encompass a range of orebody shapes, including stratabound replacement ores and hydrothermal breccias. We use the implicit method to make a detailed 3-D geological model of a stratabound IOCG in the Cloncurry district, the E1 Group, to elucidate structural controls on mineralization. This model is compared to the nearby, world-class, Ernest Henry breccia-hosted IOCG deposit. Copper mineralization in the E1 Group occurs as structurally-controlled, mainly stratabound, replacement bodies hosted in metasedimentary and metavolcaniclastic rocks intercalated with barren metaandesite. Replacement bodies in the E1 Group conform to a series of north-northwest plunging folds formed in regional D₂ during peak metamorphism. Folding was followed by local D₃ / regional D₄ shortening that formed a dextral, transpressional Riedel brittle to ductile system along the regional Cloncurry Fault Zone. Modeling suggests that much of the Cu-Au mineralization is controlled by synthetic R structures associated with this Riedel system. The deformation sequence at Ernest Henry is comparable, but differences in host rock rheology, permeability and fluid pressure may explain the variation in ore body types and total Cu-Au resource between the two deposits. The results carry implications for other districts containing these styles of IOCG mineralization. metaandesite

Introduction

Although fluid sources and genetic models for iron oxide-Cu-Au (IOCG) deposits are debated at the global scale (e.g. Barton & Johnson 2000; Hitzman 2000; Pollard 2000; Williams *et al.* 2005; Hunt *et al.* 2007; Groves *et al.* 2010), IOCGs *sensu stricto* are primarily controlled by

splays or intersections of regional faults and shear zones (Hitzman *et al.* 1992; Groves *et al.* 2010). However, knowledge about the structural controls of these deposits is less advanced than, for example, epigenetic gold deposits. A comparison between the major IOCG districts (Fig. 1) including the Gawler Craton and Cloncurry District, Australia (e.g. Oreskes & Einaudi 1990; Oreskes & Einaudi 1992; Haynes 2000; Belperio *et al.* 2007; Mark *et al.* 2006; Oliver *et al.* 2004, 2006, 2008; Rubenach *et al.* 2008; McLellan *et al.* 2010), the Fennoscandian shield, Scandinavia (Billström *et al.* 2010), Punta del Cobre, Chile (Marschik & Fontboté 2001), and Carajás, Brazil (Ronze *et al.* 2000; Grainger *et al.* 2008), reveals some similar structural settings for IOCG-style orebodies. These settings include hydrothermal breccias, veins or replacement bodies associated with the intersections between faults and shears and specific rock types, and location within dilational fault or shear jogs. Some rock types (e.g. calcareous or carbonaceous sedimentary rocks) can act as ideal chemical traps, or may focus permeability by brecciating. Fe-oxide-Cu-Au deposits appear to have formed both at relatively shallow (<5 km) depths, as in the case of Olympic Dam (Oreskes & Einaudi, 1992; Haynes *et al.* 1995), and at deeper levels (~10 km), in the case of Ernest Henry (Kendrick *et al.* 2007). Some of the major IOCG districts, such as the Fennoscandian shield, Carajás, and Cloncurry, are characterized by protracted periods of metamorphism, magmatism and metasomatism that enhance existing ores and generate new orebodies (Kirchenbaur *et al.* 2016; Macmillan *et al.* 2016; Billström *et al.* 2010; Oliver *et al.* 2008). Thus, understanding the timing of IOCG mineralization with respect to regional deformation events is critical for developing genetic models that include fluid transportation conduits and trapping mechanisms.

The Cloncurry District of northwest Queensland, Australia, hosts numerous IOCG deposits, all associated with shear zones (e.g. Baker & Laing 1998; Coward 2001; Davidson *et al.* 2002; Duncan *et al.* 2014). The recently discovered E1 Group of IOCG deposits (10.1 Mt at 0.73 % Cu, 0.22 g/t Au), located 40 km northeast of Cloncurry (Fig. 2), has not been extensively studied and may offer new insights into regional structural controls and genesis of IOCG deposits. The E1 Group is composed of three distinct orebodies: E1 North (the largest), E1 East, and E1 South. The orebodies were discovered in 1990 by Western Mining Corporation, but were not extensively drilled out until the early 2000s by EXCO Resources. The E1 Group is located 6 km east from the world-class Ernest Henry system which has total resources of 226 Mt at 1.1% Cu and 0.51 g/t Au (Rusk *et al.* 2010), and is the largest Cu-Au deposit in the Cloncurry District (Mark *et al.* 2006). The area surrounding the E1 Group and

Ernest Henry is characterized by sparse outcrop, and as a result past exploration has been heavily dependent on geophysical techniques in order to resolve regional- and deposit-scale structures that host the IOCG mineralization.

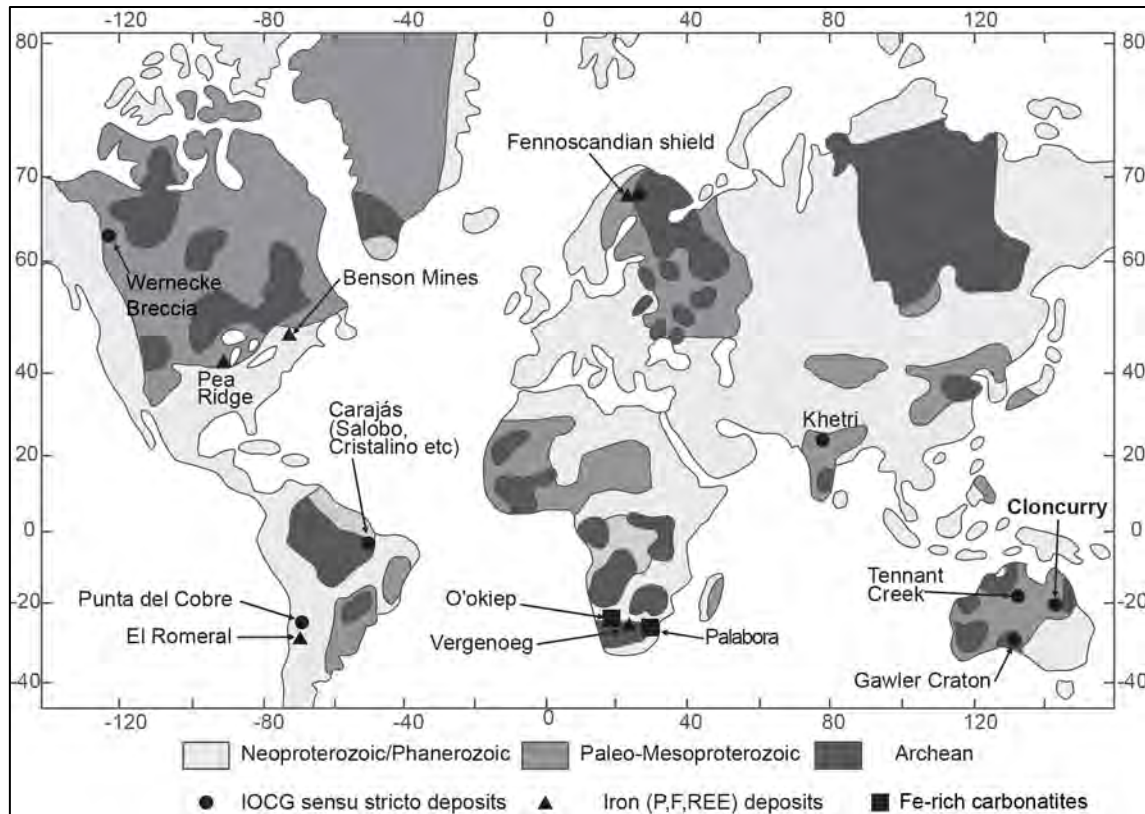


Figure 1: Global distribution of IOCG and related deposits, based on the modified map and classification scheme of Groves *et al.* (2010). Study area labelled in bold typeface. The Fennoscandian shield contains both IOCG and Iron oxide-apatite (IOA) deposits, and the symbols are placed side-by-side.

Implicit geological and geochemical modeling are powerful tools that can aid in rapid characterization of the disposition of orebodies, particularly those with limited outcrop in which cross and plan sections must be synthesized from drilling and geophysical datasets (e.g. Hill *et al.* 2014). A geological model of the E1 Group could contribute to the understanding of mineralization in this area where the subsurface geology is poorly constrained. Using 3-D modeling derived from drill core logging, open pit mapping and aeromagnetic data, this study presents the structural characteristics, deformation history, and structural controls on mineralization of the E1 Group of IOCG deposits. These aspects are compared to those of the nearby breccia-hosted Ernest Henry system in order to infer the controls on the different mineralization styles.

Regional geology

The E1 Group of IOCG deposits is located 40 km northeast of Cloncurry in the Proterozoic Mount Isa Inlier of northwest Queensland (Fig. 2). The Mount Isa Inlier is conventionally subdivided into the Western Fold Belt, Kalkadoon-Leichhardt Belt, and Eastern Fold Belt tectonic domains (Fig. 2; Blake & Stewart 1992). The Inlier is prospective for Cu, Au, Pb, Zn, Ag, U, REE, Mo, but deposit styles vary substantially between belts (Murphy *et al.* 2011). The Western Fold Belt is dominated by Mount Isa-style Cu-Pb-Zn deposits, whereas the Eastern Fold Belt and Kalkadoon-Leichhardt Belt host varying styles of Cu-Au mineralization, of which many are grouped into the IOCG classification (Williams *et al.* 2005; Groves *et al.* 2010).

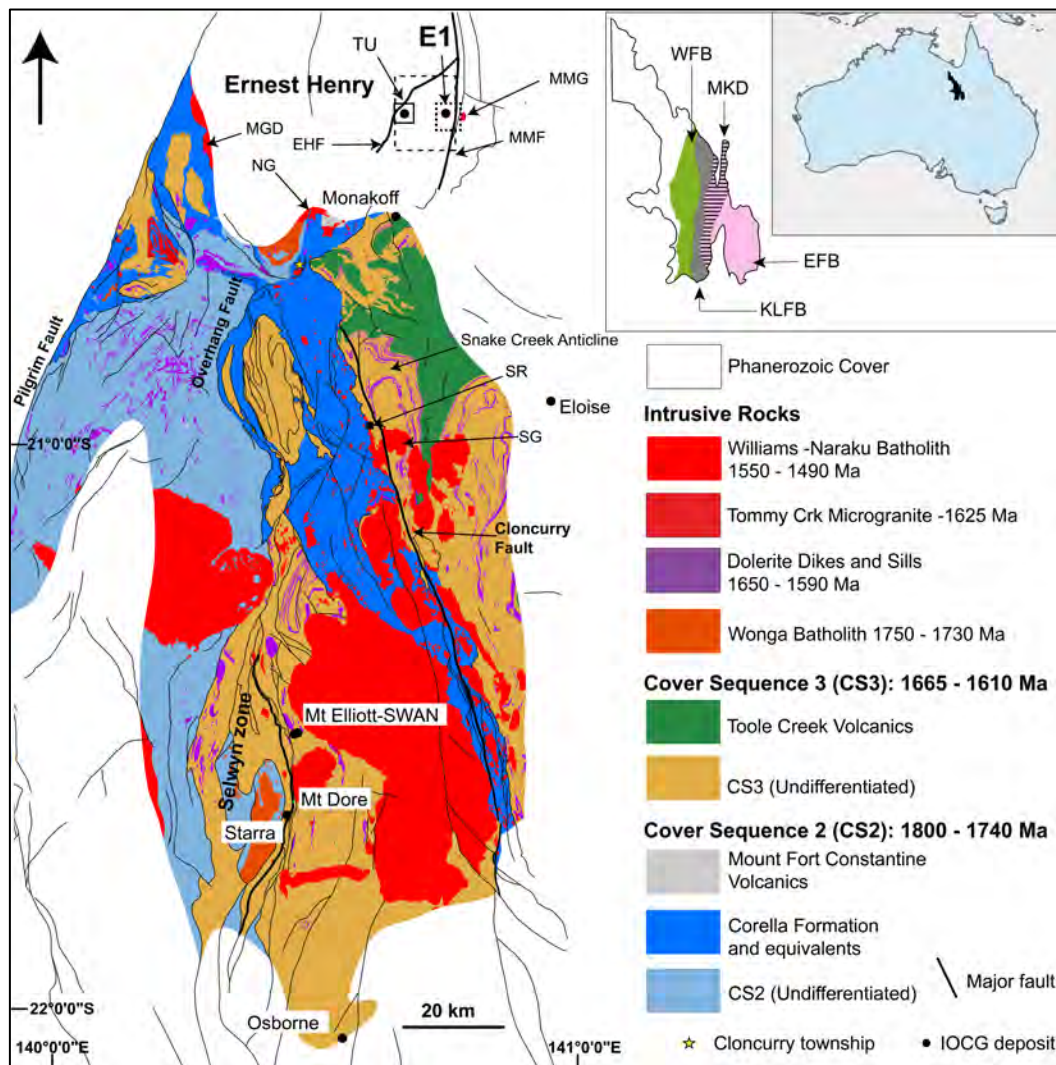


Figure 2: Interpreted bedrock geology and structures of the Eastern Fold Belt east of the Pilgrim Fault. The inset shows the major domains of the Mount Isa Inlier. Geology polygons and structure polylines are from the Geological Survey of Queensland (2011). Structures below cover were interpreted in the same report from geophysical datasets. The solid-, dashed- and dotted-outlined boxes indicate the areas represented in Figures 5, 9 and 10, respectively. EFB, Eastern Fold Belt; MKD, Mary Kathleen Domain; KLFB, Kalkadoon-Leichhardt Fold Belt; WFB, Western Fold Belt; MMG, Mount Margaret

Granite; MMF, Mount Margaret Fault; EHF, Ernest Henry Fault; MGD, Mavis Granodiorite; NG, Naraku Granite; SR, Suicide Ridge; SG, Saxby Granite.

Cover sequence deposition and early intrusions

The sedimentary and volcanic country rocks of the Eastern Fold Belt were deposited between 1875 and 1610 Ma in an intracratonic rift setting (Blake 1987 and references therein; O’Dea *et al.* 1997). They overly the *c.* 1900 Ma basement rocks of the Barramundi Orogen and are divided into three major unconformable cover sequences (Fig. 3; Page & Williams 1988; Blake & Stewart 1992).

Cover Sequence 1 (CS1), composed mostly of mafic-felsic extrusive rocks, was deposited from 1870–1840 Ma (Wyborn & Page 1983). Following a significant hiatus, mudstones, sandstones, carbonates, and evaporites of Cover Sequence 2 (CS2) were laid down between 1800 and 1690 Ma. In the area around the E1 Group and Ernest Henry, CS2 rocks are represented by the intermediate Mount Fort Constantine Volcanics and Corella Formation carbonates and siliclastic rocks; they formed synchronously from 1750–1740 Ma (Page & Sun 1998; Foster & Austin 2008). After deposition of Cover Sequence 2, granites of the *c.* 1740 Ma Wonga Batholith intruded mostly in the western portion of the Eastern Fold Belt (Wyborn *et al.* 1988). Cover Sequence 3 (CS3) sedimentary rocks and mafic volcanics were deposited between 1690 and 1650 Ma (Foster & Austin 2008; Rubenach *et al.* 2008). Mafic dykes and sills were also intruded during this time period (Rubenach *et al.* 2008). The Ernest Henry Diorite suite crystallized around 1650 Ma (Page & Sun 1998) in the region Ernest Henry. Betts & Giles (2006) and Neumann *et al.* (2006) present an alternative stratigraphic framework for the entire Mount Isa Inlier, and consider the Western and Eastern fold belts to be broadly stratigraphically correlated in the form of superbasins. Those authors have grouped the formations of Cover Sequence 2 into the Leichhardt Superbasin, while those of Cover Sequence 3 are divided into the Calvert Superbasin (Lewellyn Creek Formation-Mount Norna Quartzite) and Isa Superbasin (Toole Creek Volcanics and Staveley Formation). Similar correlations have also been proposed by Foster & Austin (2008).

Isan Orogeny: deformation and metamorphism

The post-1900 Ma deformation history of the Mount Isa Inlier is dominated by the 1650-1500 Ma Isan Orogeny (Rubenach *et al.* 2008). Deformation and metamorphism related to this orogeny is complex in the Eastern Fold Belt, and there is no consensus on the timing and number of individual events. Most studies in the Eastern Fold Belt have focused on the well-

exposed areas south and west of Cloncurry (Fig. 2) such as the Selwyn zone, Snake Creek Anticline, and Mary Kathleen Domain (e.g. Looseveld & Schreurs 1987; Adshead-Bell 1998; Rubenach & Lewthwaite 2002; Giles *et al.* 2006; O’Dea *et al.* 2006; Rubenach *et al.* 2008; Abu Sharib & Bell 2011). Those workers generally concluded that at least four major deformation events took place in the region (Fig. 3). Rubenach and Lewthwaite (2002) and Giles *et al.* (2006) describe an early (1680-1640 Ma, Rubenach *et al.* 2008) extension-related event (denoted D_{bp} by Rubenach *et al.* 2008), resulting in a bedding subparallel foliation (Fig. 3). This extensional event was followed by three or four major crustal shortening events (Mark *et al.* 2000; Blenkinsop *et al.* 2008; Rubenach *et al.* 2008; Abu Sharib & Bell, 2011).

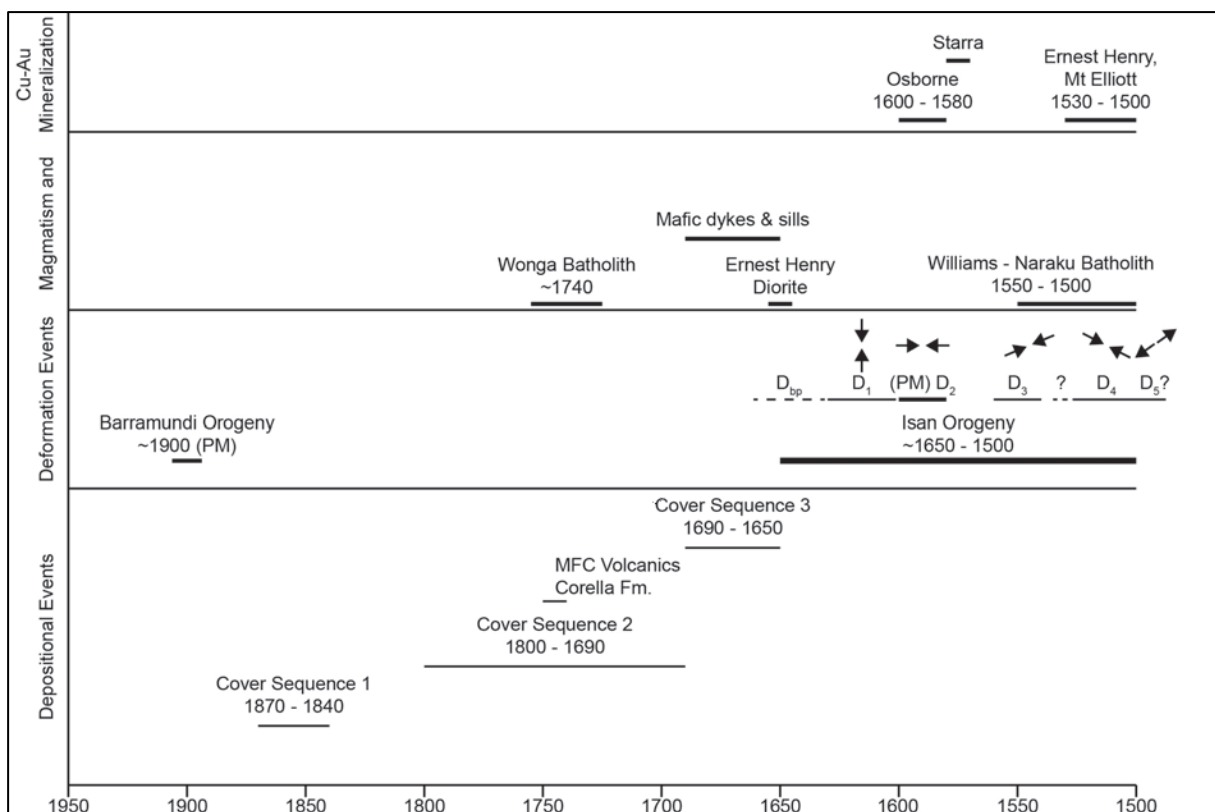


Figure 3: Diagram showing the major depositional, deformation, magmatic and mineralization events in the Eastern Fold Belt of the Mount Isa Inlier after 1800 Ma. See text for references. PM, Peak metamorphism.

The D_1 event (1630–1600 Ma; Rubenach *et al.* 2008) is poorly preserved, and is characterized by east-west folds and steep, east-west S_1 foliation (Bell 1983; Adshead-Bell 1998; Bell & Hickey 1998; Rubenach & Lethwaite 2002; O’Dea *et al.* 2006; Rubenach *et al.* 2008). The dominant north-south-trending, steep, and upright to vertical folds and fabric recognizable widely throughout the Mount Isa Inlier resulted from the D_2 (1600–1580) event at amphibolite facies peak metamorphic conditions (Page & Sun 1998; Giles & Nutman 2002; Foster & Rubenach 2006; Rubenach *et al.* 2008). This was followed by D_3 (1550 Ma; Page &

Sun 1998; Rubenach *et al.* 2008; Duncan *et al.* 2011) which is characterized by north-northwest-trending folds with steeply dipping axial surfaces and penetrative crenulation of S₂ (Rubenach *et al.* 2008).. Northeast-trending folds with steep axial surfaces are considered by Rubenach *et al.* (2008) to be a late D₄ event synchronous with intrusion of the c. 1527 Ma Saxby Granite; D₄ may have continued until ~1500 Ma (Davis *et al.* 2001; Duncan *et al.* 2011). Some authors (e.g. Beardsmore 1992; Austin and Blenkinsop 2010) have described an even later (≤1500 Ma) dominantly brittle event (D₅) characterized by southwest-northeast extension. Major regional structures such as the Cloncurry and Pilgrim faults (Fig. 2) likely originated as basin-bounding faults during extensions that were subsequently reactivated as reverse or transform structures during the Isan Orogeny (Blenkinsop *et al.* 2008; Austin & Blenkinsop 2010).

Due to poor outcrop, deformation in the area northeast of Cloncurry has not been extensively studied, except at isolated deposits such as Ernest Henry (Twyerould 1997; Mark *et al.* 2000; Coward 2001). Figure 4 displays the local deformation schemes interpreted by these authors as correlated to the regional deformation history south of Cloncurry.

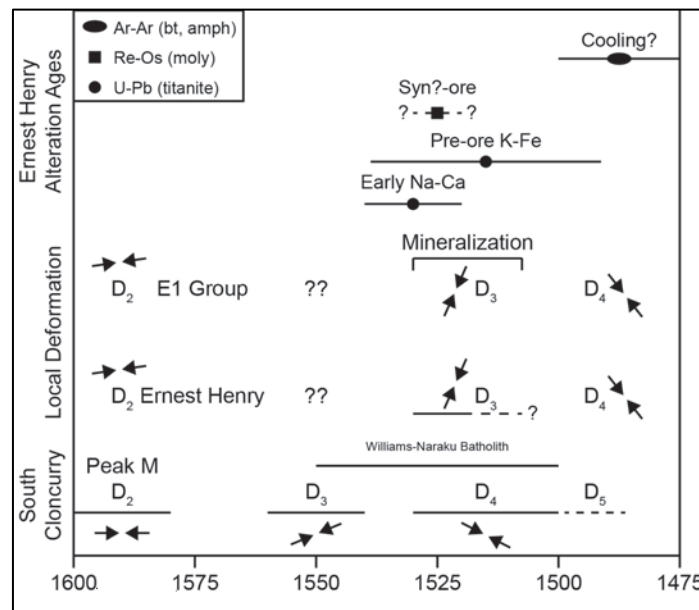


Figure 4: A comparison of reported local deformation schemes at Ernest Henry and the E1 Group, with the regional events shown in Figure 3. See text for references.

The Ernest Henry deposit is characterized by northeast-trending brittle to ductile zones (Fig. 5a) that are splays of a regional northeast-southwest structure, known as the Ernest Henry Fault (Fig. 1). Twyerould (1997) interpreted mineralization to be of regional D₃ or D₄ timing (Fig. 4), and in a compressional setting. The shear zones may be focused around the hinge of

a northeast-plunging fold developed in D₂ (Twyerould 1997). Coward (2001) conducted a detailed structural study of the system and interpreted the northeast-trending structures of the area to have formed during local D₂, including the shear zones which bound the ore breccia (Fig. 5a). These shears were reactivated and overprinted by local D₃ extensional shearing during mineralization. The local D₄ event was dominated by brittle reactivation of D₃ faults. Mark *et al.* (2006) recognized only the D₁-D₃ events, and correlated them directly to the regional sequence; they interpreted mineralization as syn-D₃.

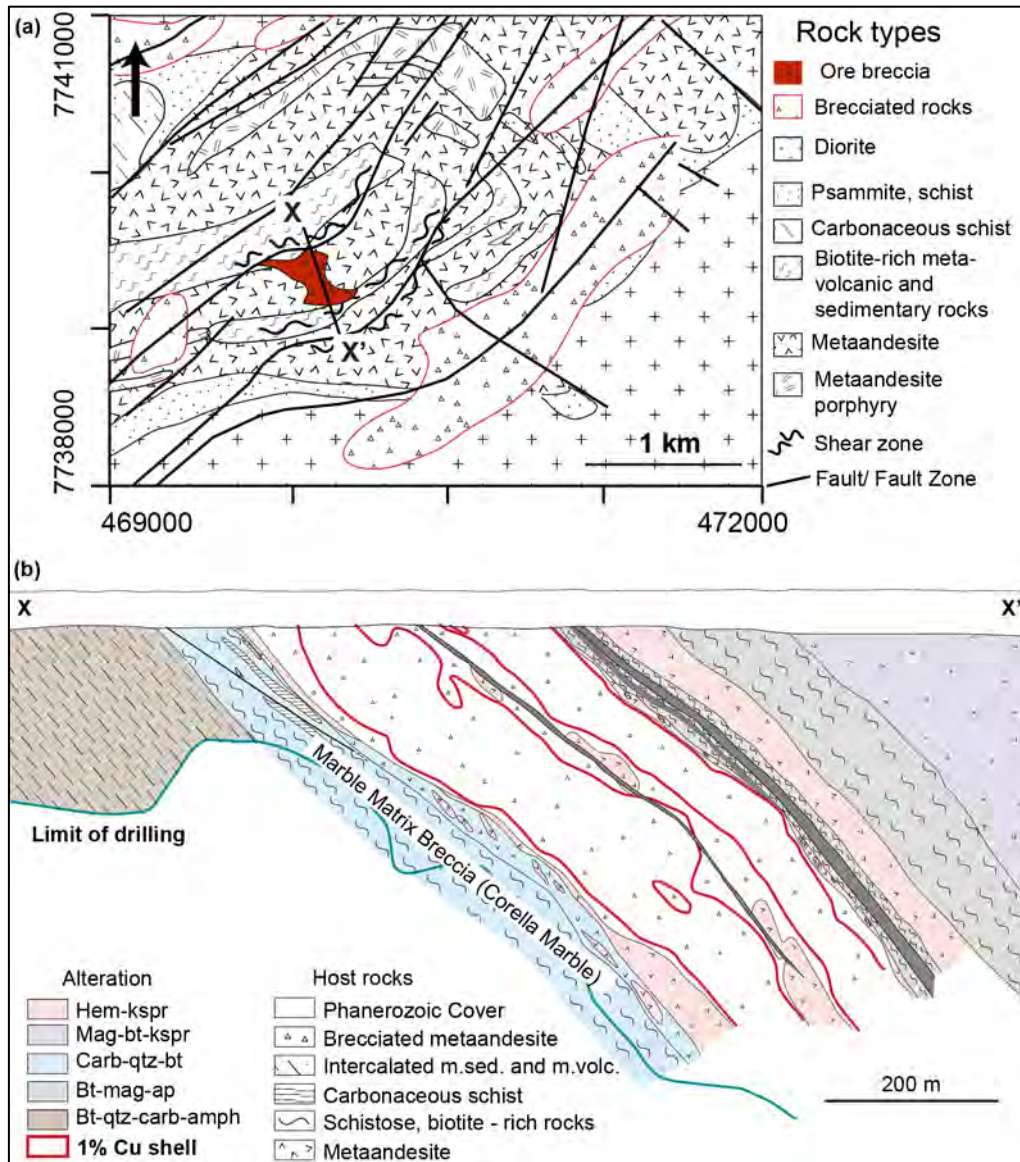


Figure 5: Geological map and cross section of the Ernest Henry IOCG deposit. (a) Plan view (c. -50 m Above Sea Level (ASL)) composite based on Twyerould (1997) and Mark *et al.* (2006). (a) Long section through the orebody modified, with permission, from Coward (2001). Rock type groupings vary between authors. The strongly-foliated, biotite-rich, rocks in plan section (a) correspond with the metasedimentary and metavolcanic rocks in (b). Brecciated rocks in (a) include fractured equivalents of all other rock types.

Late intrusions and IOCG mineralization

Following peak metamorphism in the Isan Orogeny, voluminous A-type granitoids of the Williams-Naraku Batholith (1550–1500 Ma; Fig. 3) intruded throughout the Eastern Fold Belt (Page & Sun 1997). The closest Williams-Naraku intrusion to the E1 Group is the Mount Margaret Granite, 2 km east of the deposits (Fig. 2); it is dated at 1530 Ma (Page & Sun 1998). No other granites are spatially associated with Ernest Henry or the E1 Group; the nearest other granite pluton, the Naraku Granite, crops out 20 km southwest (Fig. 2). IOCG-style mineralization in the Mount Isa inlier occurred over *c.* 100 Ma (1595–1500 Ma): Osborne formed during peak metamorphism at *c.* 1595 Ma (Gauthier *et al.* 2001) and Starra at 1568 ± 7 Ma (Duncan *et al.* 2011). Both deposits are interpreted to have formed from metamorphic fluids (Fisher & Kendrick 2007; Duncan *et al.* 2011). Other IOCGs in the district, such as Ernest Henry and Mount Elliott, formed much later between 1530–1500 Ma (Wang & Williams 2001; Mark *et al.* 2006; Duncan *et al.* 2011), overlapping with intrusion of the Williams-Naraku Batholith. These granites have been postulated as one potential source of Cu-Au-bearing fluids for the younger IOCGs (Kendrick *et al.* 2007; Oliver *et al.* 2008; Williams *et al.* 2014).

Host rocks and paragenetic sequence of the E1 Group

The E1 Group is hosted in a sequence of metasedimentary rocks intercalated with intermediate metavolcanic rocks. The host rocks do not crop out and are unconformably overlain by 30 – 50 m of Mesozoic sedimentary rocks. The metasedimentary rocks are composed of marbles, psammites, and carbonaceous metasiltsstones and pelites (Fig. 6a-e). The metavolcanic rocks consist of basaltic metaandesite to metaandesite with variable porphyritic, amygdaloidal and massive textures, as well as metavolcanic breccia and metatuff. The rocks are similar to those that host the nearby Ernest Henry deposit: the 1750 – 1740 Ma Mount Fort Constantine Volcanics and Corella Formation of upper Cover Sequence 2 (e.g. Foster and Austin 2008). This metavolcano-sedimentary package is intruded by diorite (Fig. 6f), which is likely related to the Ernest Henry Diorite suite (*c.* 1650 Ma; Page & Sun 1998). Clasts of the diorite are present in albite-hematite-K-feldspar-biotite-altered, discordant, breccia (Fig. 6g-i), that cross-cuts the system (Fig. 6i). The discordant breccia is intruded by

dolerite dykes of unconstrained age (Fig. 6j). Ores are hosted primarily in the metasedimentary rocks (excluding the carbonaceous pelite), but strongly-sheared metavolcanic rocks are also mineralized in the E1 North Shear zone.

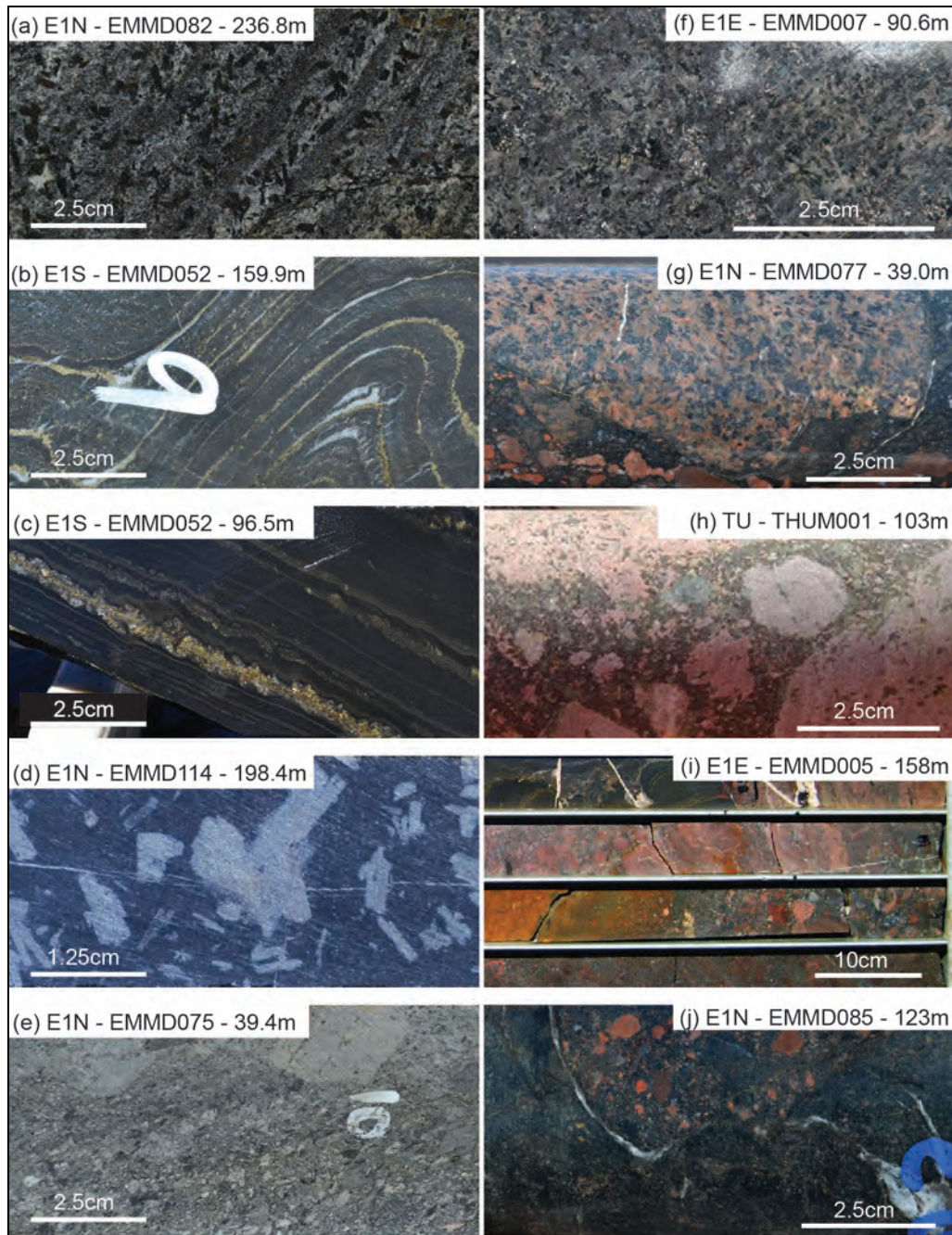


Figure 6: Drill core photographs of E1 Group host rocks. (a) Porphyroblastic marble with disseminated magnetite and sulphide alteration. Porphyroblasts are chlorite after actinolite. (b) Carbonaceous metasiltstone with pyrite-carbonate-quartz alteration and veining. Note dilational fold microreefs infilled with carbonate and quartz. (c) Carbonaceous schist/phyllite with similar pyrite-carbonate-quartz alteration. (d) Representative plagioclase-phyric metaandesite in the metavolcanic rocks above and below the marble unit in Fig. 8. Note slight albite(-hematite) alteration of phenocrysts. (e) Metatuff. (f) Diorite inferred to be from the Ernest Henry Diorite suite. (g) Diorite clast in discordant breccia. (h) Less altered discordant breccia from Third Umpire prospect north of Ernest Henry. Matrix composed mainly of albite, amphibole and pyroxene. (i) Discordant contact of metasiltstone (upper right part of core tray) with discordant breccia. (j) Dolerite with discordant breccia xenoliths. E1N, E1 North; E1E, E1 East; E1S, E1 South. Act, actinolite; Cal, calcite; Py, pyrite; Qz, quartz; Bt, biotite; Chl, chlorite; Ab, albite; K-spar, K-feldspar; Px, pyroxene; Dol, dolerite.

Mineralization at the E1 Group is characterized by layer-controlled replacement of the metasedimentary rocks, accompanied by relatively minor veining (Fig. 7). Alteration and mineralization can be described in three major phases (Fig. 7): early albitization (Fig. 7a), pre-ore magnetite-apatite-biotite-K-feldspar (Fig. 7b), and ore-stage carbonate-chalcopyrite-barite-fluorite-magnetite (Fig. 7c). This sequence is comparable to that of the nearby Ernest Henry deposit, which suggests similar chemistry of the mineralizing fluid(s) in both deposits. However, such similarity does not necessarily indicate a common origin.

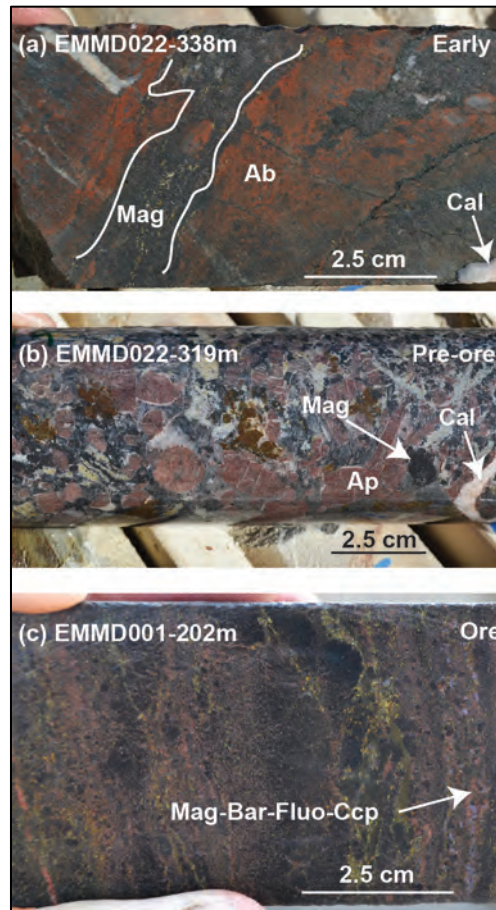


Figure 7: Alteration paragenesis of the E1 Group. (a) Early albite (hematite dusting imparts red colour) alteration overprinted by magnetite and sulphides. Albitization is prevalent throughout the region and its relationship to mineralization is unclear. (b) Pre-ore magnetite-apatite-carbonate alteration with pyrite and minor chalcopyrite overprints. This stage is associated with abundant biotite \pm K-feldspar \pm quartz in other examples. (c) Fine-grained, ore-stage barite-fluorite-carbonate-chalcopyrite-pyrite alteration associated with shear fabrics in marble? Mag, magnetite; Ab, albite; Cal, calcite; Bar, barite; Fluo, fluorite; Ccp, chalcopyrite.

3-D geological modeling

The development of three-dimensional (3-D) implicit modeling software in the last decade has provided geologists with new means for quickly visualizing the geology of mineralized systems in 3-D space (e.g. Cowan 2003; Alcaraz *et al.* 2011; Hill *et al.* 2014; Stewart *et al.* 2014). The E1 Group represents an ideal study area to conduct implicit modeling, as

substantial assay and core photo databases are available to characterize the subsurface geology.

Datasets

A 3-D geological model of the E1 Group was generated from a combination of diamond drill hole (DDH) logging, open pit mapping, and ground and aerial magnetic surveys (Figs. 8-10). Twenty-three diamond holes were physically logged and observations from these holes were used to log lithologies of remaining 260 diamond holes using the core photo database. Geophysical datasets were provided by the mine operator and include a regional aerial magnetic survey with 50 m flight and 500 m tie-line spacing (Fig. 9), as well as a ground magnetic survey across the E1 Group with 50 m line spacing (Fig. 10). All drill hole and geophysical datasets were converted to GDA 94 projection.

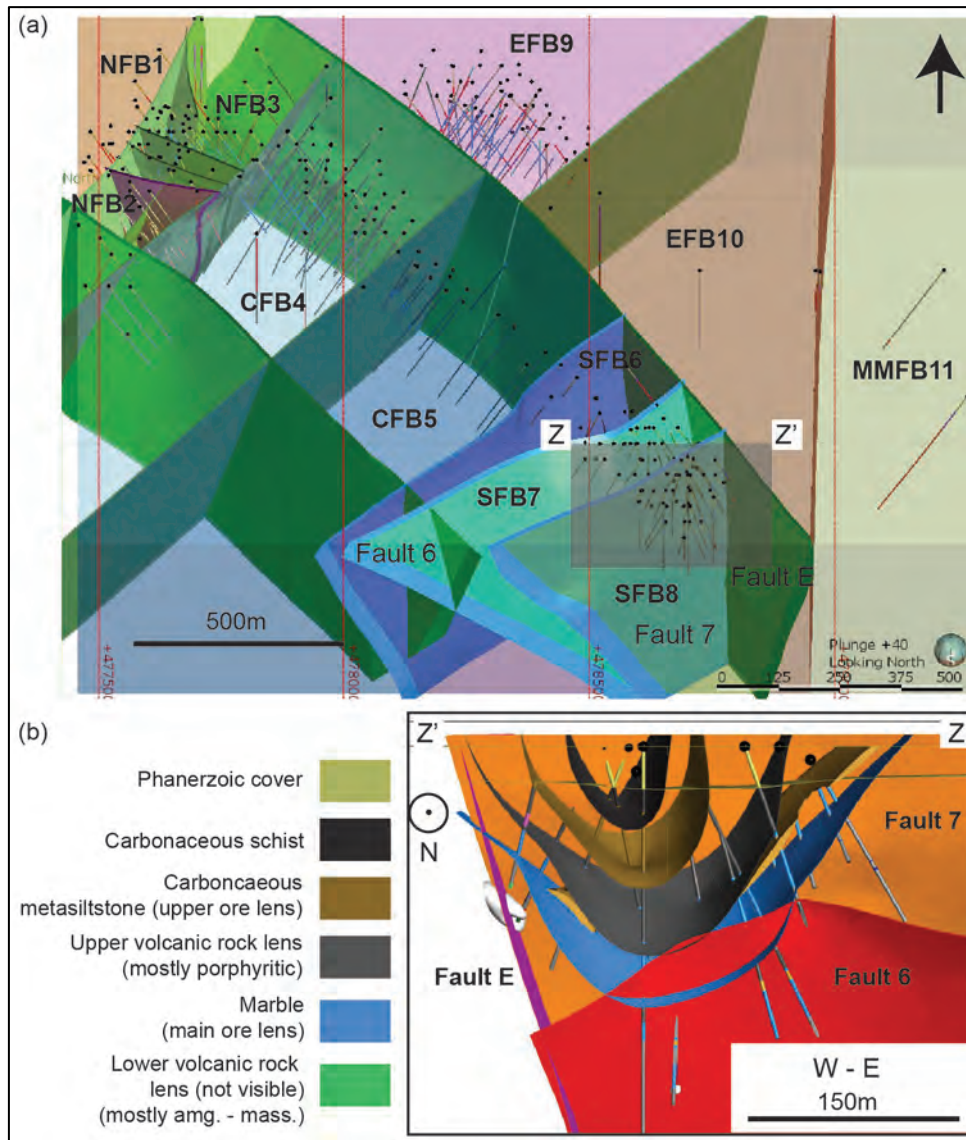


Figure 8: (a) Rendered image of the diamond drill hole dataset used for geological modelling, along with the modeled 'Fault Block' volumes generated from interpreted faults (see Fig. 11). Geochemical modeling parameters vary for each fault block (see Table 1). (b) Vertical, west-east cross section of the E1 South synform (location shown in (a)), showing an example of isosurfacing in the South fault blocks with the 'Stratigraphy' function in Leapfrog (isosurfaces are not shown in (a)). See Fig. 6 for host rock descriptions. FB, fault block; N, north; S, south; E, east; C, central; MM, Mount Margaret.

Geological Modeling Parameters

Geological and numerical geochemical modeling were conducted in Leapfrog Geo 2. Geological contact surfaces for the metasedimentary and metavolcanic rock sequence were modeled using the Stratigraphic Sequence function (Fig. 8B). Discontinuous metatuff lenses in this stratigraphy were modeled as veins. The diorite, discordant breccia, and dolerite lithologies were modeled in that order as intrusions crosscutting the stratigraphy. Extensive shearing and metasomatism in the western portion of the E1 North orebody has obscured clear identification of protoliths; as a result, some of the rocks in this area were classified as 'sheared sedimentary rocks' (Fig. 11) when continuous layering was observed, or as 'sheared

sedimentary and volcanic rocks' when layering was discontinuous or relict volcanic textures were observed (Fig. 11). The discordant nature of the shear zones necessitated modeling of these zones as intrusions, and structural anisotropic trends were applied to the shear zones in order to accurately represent their orientations. The model was subdivided into 11 fault blocks (Fig. 8A). A cutaway of the model is displayed in Figure 12.

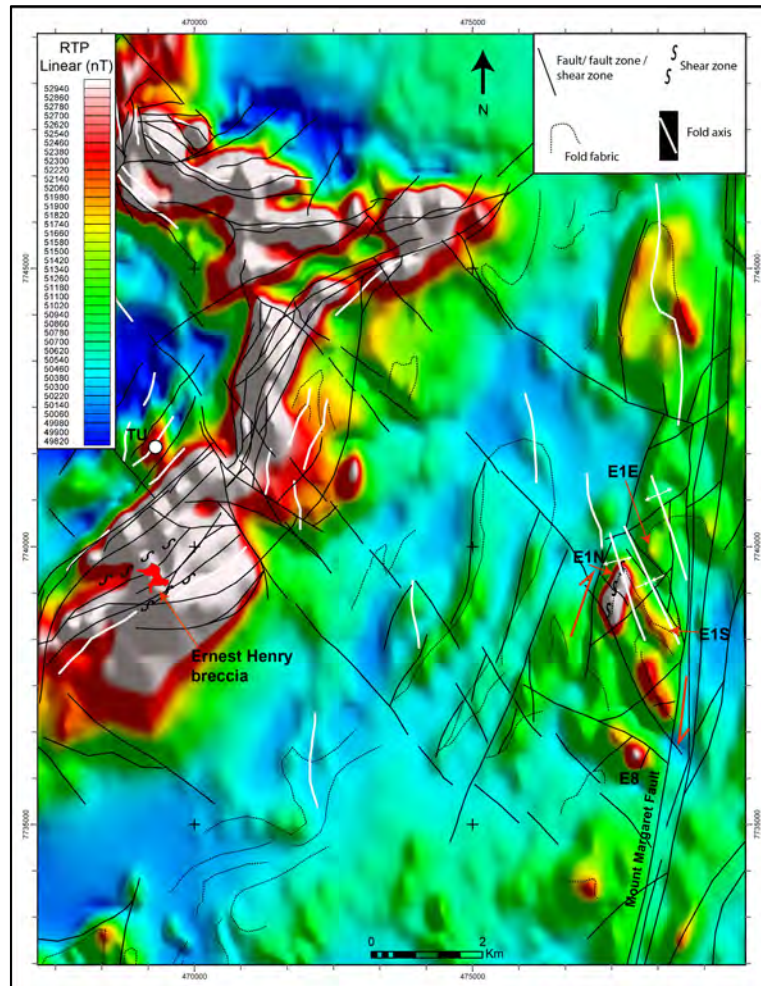


Figure 9: Structural interpretation of the Ernest Henry-E1 Group area. Reduced to Pole (RTP) aerial Total Magnetic Intensity (TMI) image. Data from Xstrata Copper Exploration (Glencore). Converted to GDA 94 projection.

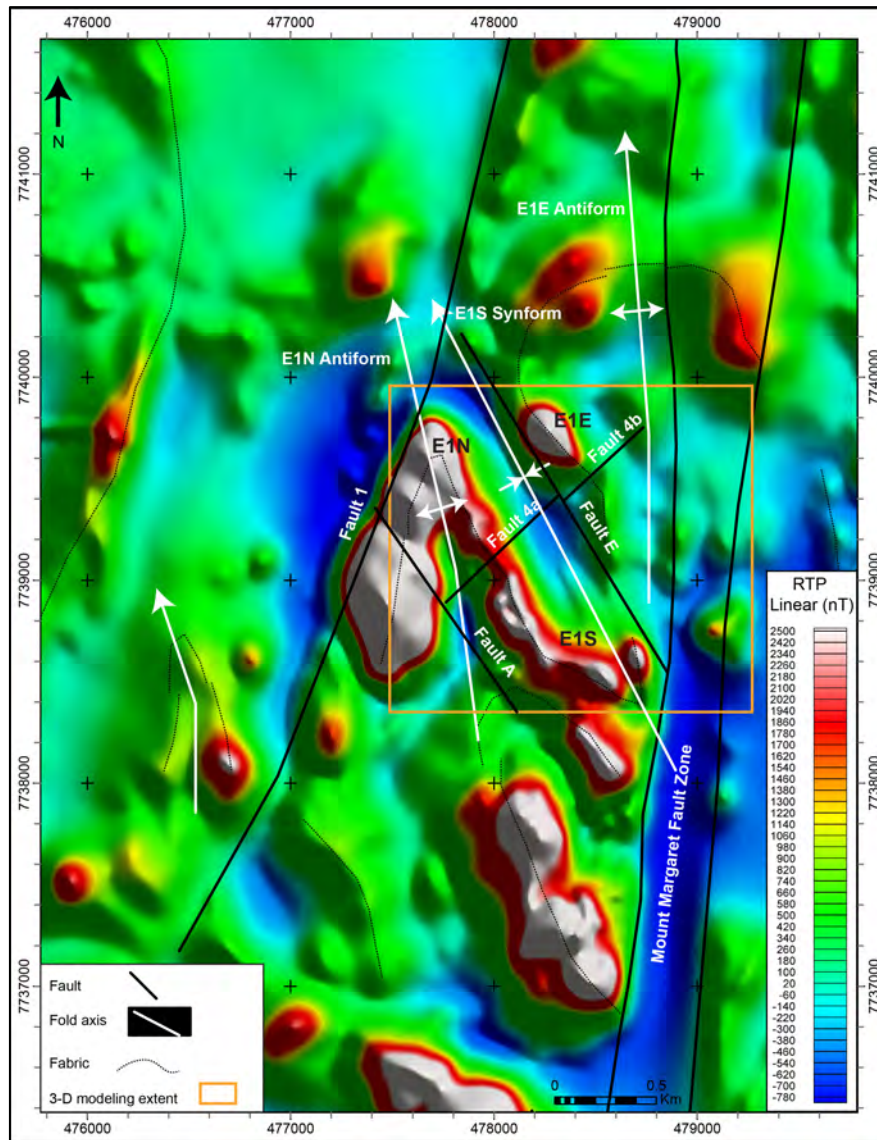


Figure 10: Structural interpretation of E1 Group area. Based on RTP aerial TMI survey conducted using 50 m flight line and 500 m tie-line spacing with 25 m clearance. Data from Xstrata Copper Exploration (Glencore), and converted to Geocentric Datum of Australia (GDA) 94 projection. E1N, E1 North; E1S, E1 South; E1E, E1 East.

E1 structural geology

The E1 Group does not outcrop, and as a result the understanding of its structures comes mostly from 3-D modeling derived from drill core and limited mapping of the orebody periphery in the E1 North open pit.

Deposit geometry and macrostructures

The topography of the Proterozoic-Mesozoic unconformity forms a *c.* 10 m culmination over the E1 North orebody. The general geometry of the E1 Group orebody is characterized by northwest- to north-northwest plunging similar, open folds with near-vertical axial surfaces (Figs. 11-13). E1 North is hosted near the hinge of a north-northwest-plunging antiform, and

the eastern limb of the antiform transitions into the west limb of the northwest-plunging E1 South synform which contains the E1 South orebody. The metasedimentary rock layers thin substantially on the limb connecting the folds, and the marble layer appears to pinch out on the west limb of the E1 North Antiform although it may be obscured by the intense shearing and metasomatism in that zone. Drilling indicates that the E1 East orebody dips steeply to the east, and regional aerial magnetic data suggest that this structure forms the overturned southwest limb of the north-northwest-plunging E1 East antiform (Fig. 10). This antiform continues from the east limb of the E1 South synform and the thickness of the metasedimentary rocks increases. The metavolcanic sequence present between the marble and metasilstone units at E1 North and South is mostly absent at E1 East with the exception of some isolated pods of porphyritic metavolcanic rocks.

The E1 North Antiform is cross-cut by a series of northeast-trending, northwest-dipping, brittle – ductile shear zones collectively referred to as the E1 North Shear Zone (Figs. 14, 15a-b). The most intense shearing in this zone is mostly developed in marble, metatuff and metavolcanic breccias, but some shear fabric is also developed in the coherent porphyritic and amygdaloidal metavolcanic rocks (Figs 3a, 18c). A combination of high strain and metasomatism associated with the E1 North Shear Zone, coupled with significantly deeper weathering, have inhibited clear protolith identification within some portion of the shear zone (Figs. 16b, 18c). As a result, it is not certain whether the Corella Marble horizon pinches out on the west limb of the antiform, or is simply obscured by alteration and shear fabrics. Drill core observations from within the shear zone yield shear senses in multiple directions, causing ambiguity regarding the deposit-scale sense of movement. However, an isolated lens of mineralized Corella Marble adjacent to the main lens probably moved down and to the west with respect to the main horizon, suggesting a normal component of shear.

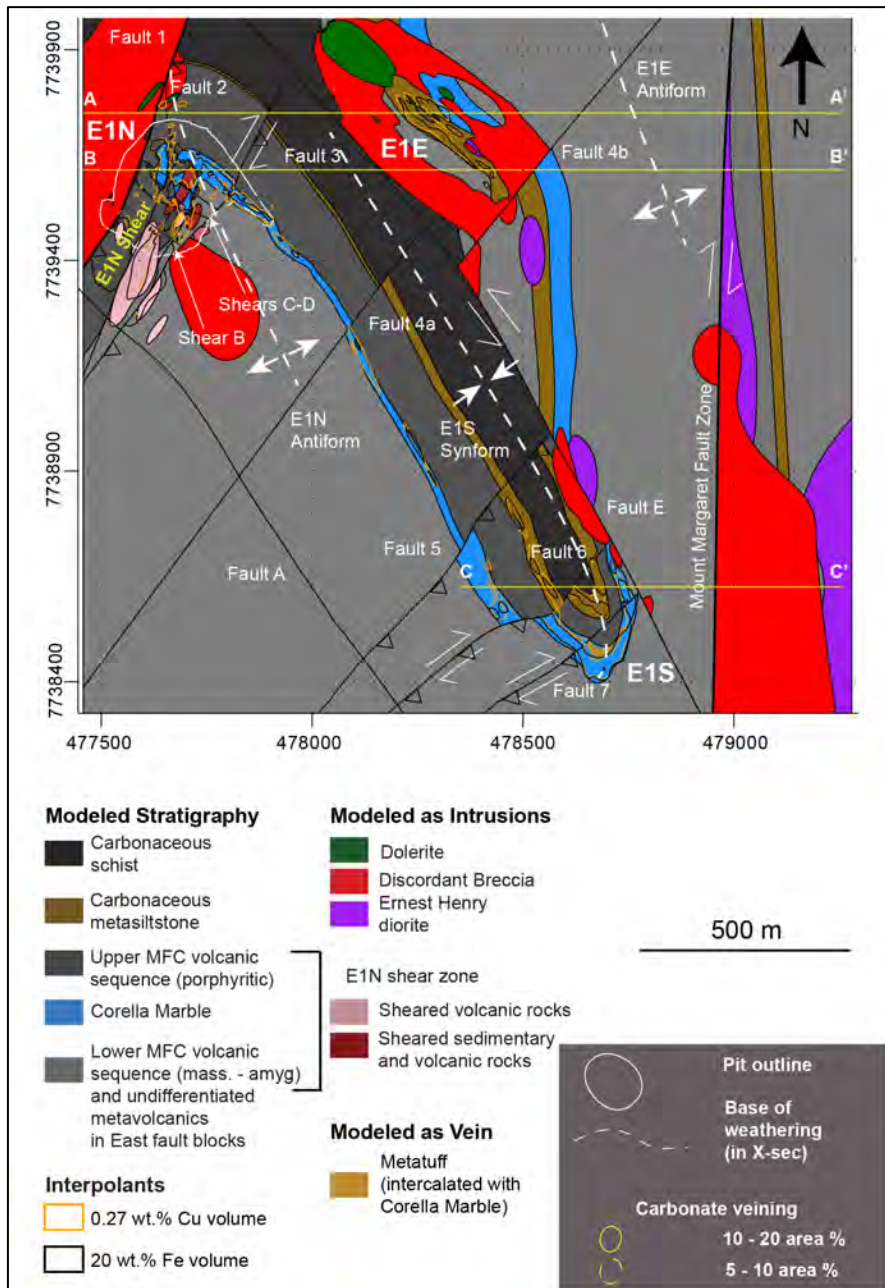


Figure 11: 75m ASL plan section of the E1 Group rendered from the 3-D geological model (extend shown in Fig. 10), showing the rock types, major folds, faults, and shear zones of the E1 Group. The metatuff is conformable, but was modeled as a 'Vein' in the Leapfrog software because of its lateral discontinuity. Copper and iron outlines are sections rendered from the modeling interpolants in Fig. 19.

The E1 North Shear Zone is coincident with mineralization and, southwest of the orebody, alteration in the shears transitions from laminated magnetite-barite-fluorite-chalcopyrite ore into massive magnetite ± apatite ± pyrite (Fig.7b, 15). Three northwest-trending structures (Shear zones B-D; Fig. 11), dipping ~70° northeast and nearly perpendicular to the E1 North Shear Zone, are interpreted to represent conjugate brittle-ductile shear zones. The conjugate structures are also coincident with mineralization observed in the open pit (Fig. 14a) and

modeled Cu-Fe mineralization (see next section; Fig. 15). The presence of these conjugate shear zones implies a component of strike-slip movement in the E1 North Shear Zone. The Shear Zone and its conjugate shear zones are bounded by parallel northeast-trending faults with variable dip-slip and strike-slip components (Figs. 14d, 15a-b). The faults coincide with changes in rheology caused by abrupt shifts from magnetite dominated to albite-quartz dominated alteration. These faults, shear zones, and the E1 North Shear Zone are considered to collectively represent a single brittle-ductile deformation system, with the brittle strain focused mostly in more competent rocks. Fault 1 dips steeply southeast at 85°, while Faults 2 and 3 dip 60°–70° northwest. Fault 1 is clearly traceable in reduced to pole total magnetic intensity (RTP-TMI) for over 2 km north and south of E1 North. Modeling indicates reverse net slip of up to 20 m along these faults. Fault 3 is also characterized by *c.* 20 m of dextral movement.

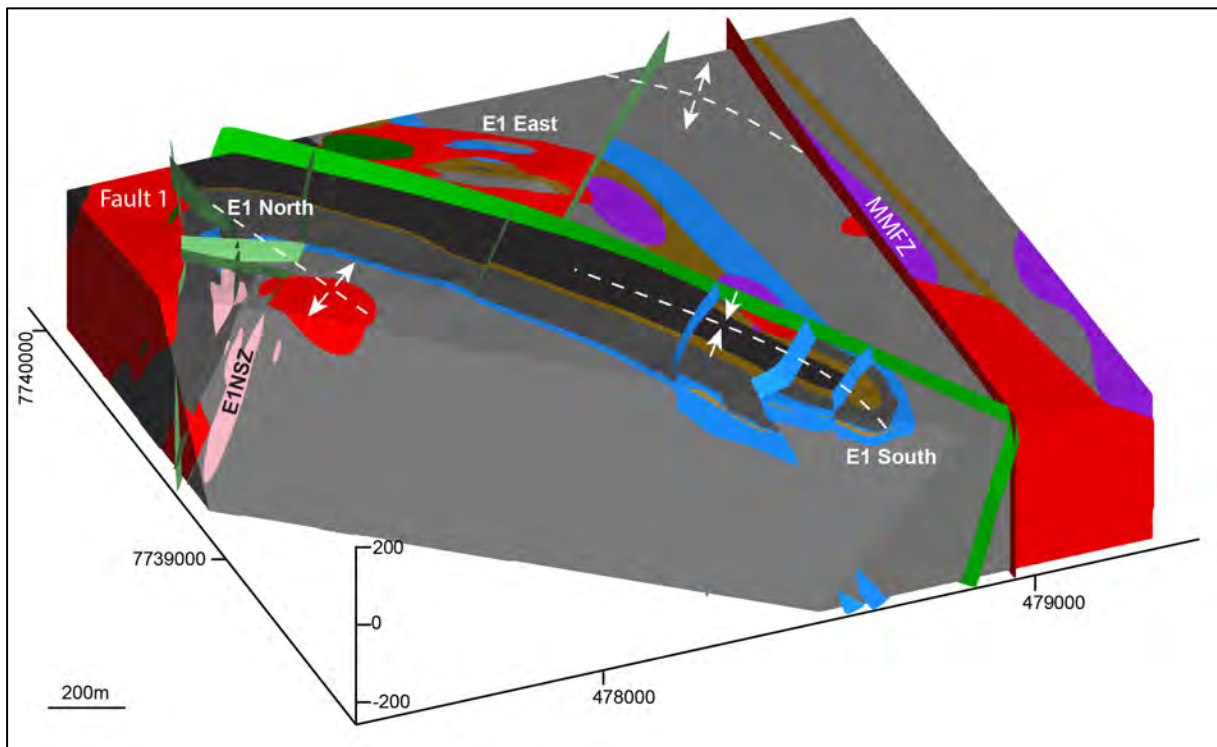


Figure 12: Three-dimensional cutaway of E1 Group 3-D geological model, showing the major D₂ folds that define the E1 North and E1 South orebody geometries. Red faults are D₂ or earlier. Green faults are (local) D₃ and later. Blue faults are (local) D₄ and later. Vertical axis is elevation ASL (m). See Fig. 8 for legend.

E1 South Faults 5–7 (Fig. 11; 15d) exhibit reverse and strike-slip separation, and dip from ~80° to 60° to the southeast. Bends in Faults 5 and 6 are interpreted to have been caused by rheological contrast between the ductile marble and brittle coherent metavolcanic layers. Unlike the E1 North faults, these structures do not coincide with high Cu-Fe concentrations or shear zones, and they offset all alteration. A major NW-SE trending fault (Fault E; Fig. 11)

separates E1 East from E1 North and South. Truncation of the metasedimentary rock horizon hosting the E1 East and E1 South orebodies by Fault E suggests strike-slip movement along this structure. Fault A (Fig. 11) is inferred mainly from aeromagnetics and its offset is not clear. Faults 4a and 4b likely represent a single northeast-southwest structure offset by Fault E.

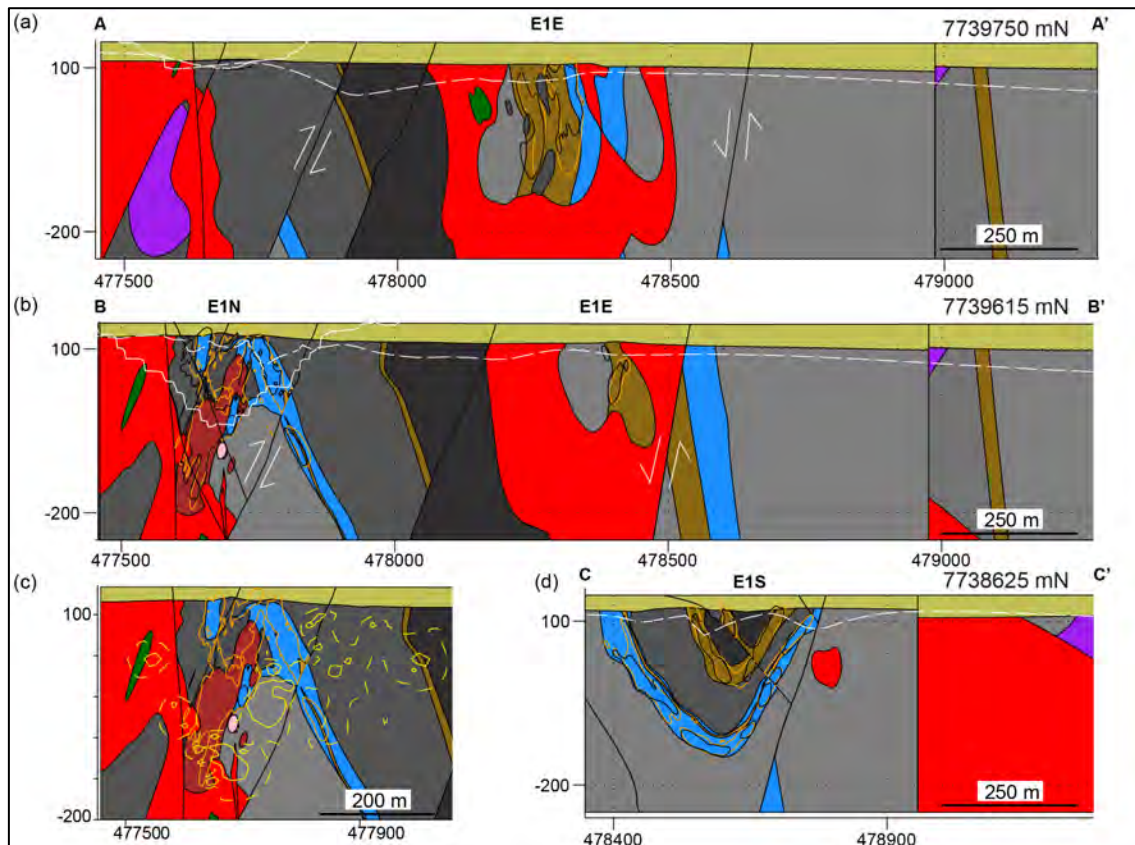


Figure 13: Cross sections of the E1 Group Geological model along lines shown in Fig. 8. (a) A-A', E1 East. (b) B-B', E1 North. (c) Inset of B-B' showing contours of abundance of carbonate veining. (d) C-C', E1 South. Vertical axis is elevation ASL (m). See Fig. 8 for legend.

The detailed structure of E1 East is not well-constrained, but core logging indicates that the metasedimentary rocks are strongly sheared throughout the system. Without surface exposure the scale and sense of the shearing is not clear. Initial Cu-Fe interpolants at E1 East follow the distribution and attitude of the metasedimentary rocks, and no northeast-trending structures are apparent, suggesting that the E1 East shear zone is parallel to the northwest-trending limb of the E1 East Antiform. The Upper Volcanics layer (Figs. 8, 11) which separates the Corella Marble and metasiltstone horizons at E1 South is mostly absent at E1 East, and the entire metasedimentary rock sequence is nearly twice as thick at E1 South. Isolated pods (> 20 m) of cohesive metavolcanic rocks within the metasedimentary rocks at E1 North and East

(texturally identical to the continuous sequences) may represent large-scale boudins within this shear zone (Fig. 15c).

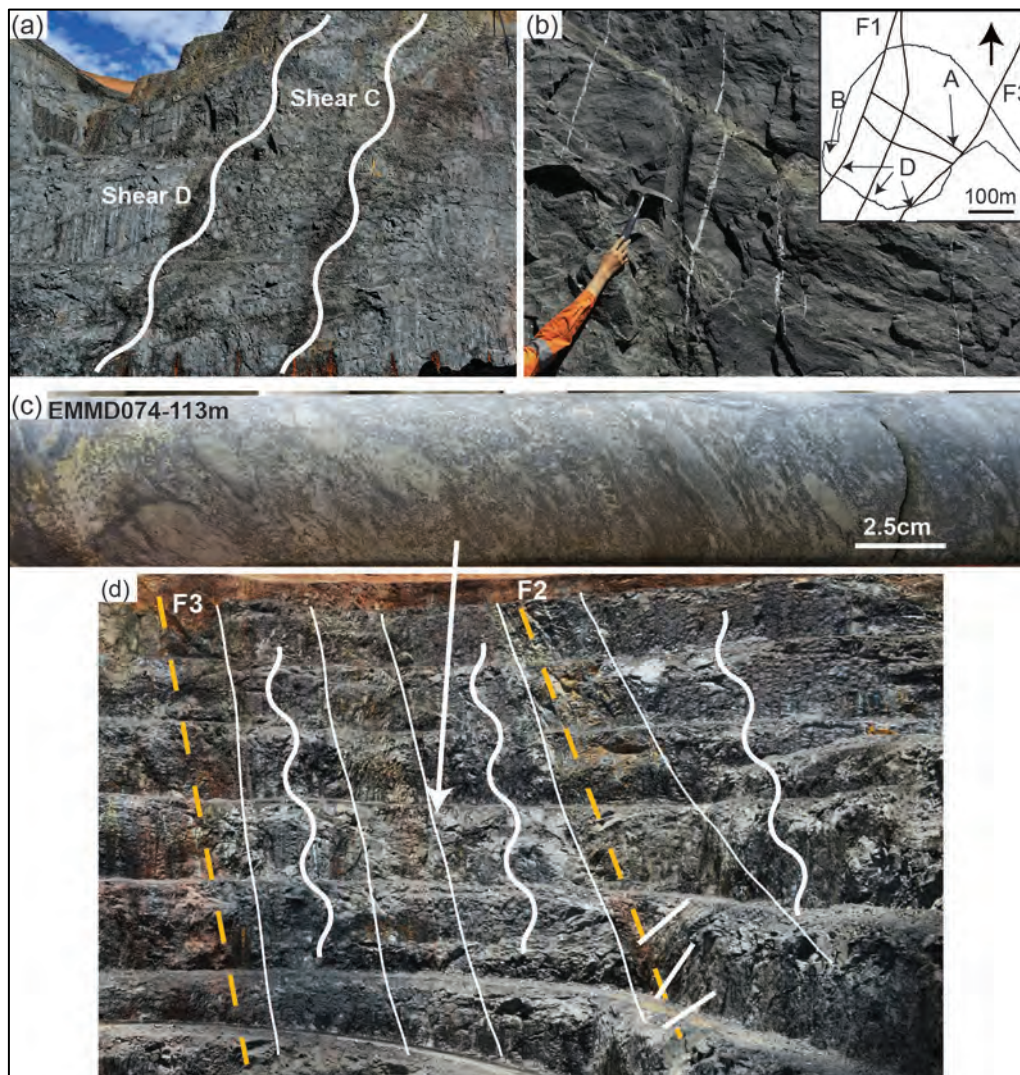


Figure 14: E1 North fault and shear structures visible in the E1 North open pit. (a) Fault/shear zones C and D (see Fig. 8). Dark material is magnetite alteration. (b) Sub-vertical carbonate±fluorite±barite±sulfide tension veins near Fault 1. (c) Photograph of a drill core intersection of sheared metavolcanic breccia in the E1 North Shear Zone. (d) Three magnetite-pyrite-apatite-altered shear zones (white outline) of the E1N Shear Zone exposed in the southwest wall of the E1 North open pit. Arrow indicates approximate location of the drill core intersect in (c). These correspond to the modelled linear zones of high (□ 20%) Fe shown in Fig. 5b. Purple lines indicate *c.* 45° dipping carbonate veins associated with Fault 2. The orientation of these veins and those in (b) suggest extensional or normal movement along the faults and shear zones.

Meso- and micro-scale structures

Ductile structures are prevalent in metasedimentary rocks throughout the study area. Close to open, asymmetric folds with < 10 cm to > 10 m wavelengths are common. The northwest-southeast to southwest trend of their axial surfaces (Fig. 17b) is consistent with that of the E1 North Antiform and E1 South Synform and they are considered to be parasitic. The 30-60° dip of the axial surfaces may be due to refolding (see Deformation sequence below). Sporadic flaser cross-bedding found in E1 East metasedimentary rocks indicates that some bedding is

locally overturned by folding, but this has not been correlated to the entire E1 East orebody. Differential folding of siliceous and pelitic layers within the metasilstone has formed dilational zones in the fold hinges infilled with carbonate, quartz and sulfide (Fig. 6b). Microfaulting is abundant in the metasedimentary rocks and is typically associated with boudinage of siliceous layers in between calcareous and pelitic layers. Boudin geometry and strain at the drill core scale are variable, with thicker beds necked by relatively narrow (< 5 cm) veins (Fig. 16b) and others completely fragmented into breccia-like textures surrounded by shear fabric. These pseudo-breccia textures are similar to those observed in the Marble Matrix Breccia at Ernest Henry (Twyerould 1997; Marshall & Oliver 2008), and are common in the Corella Formation throughout the Eastern Fold Belt. The boudins are typically sheared and imbricated. Foliation is widespread across the E1 Group and is generally restricted to metasedimentary rocks except in high-strain zones like the E1 North Shear Zone. The foliation is defined by mica but in highly-mineralized zones it is defined by sulfide and magnetite alteration. Kinematic indicators in coarse-grained clastic rocks (Fig. 16b) indicate that much of this foliation in the E1 North Shear zone formed by shearing, but the nature of foliation in marble and other metasedimentary rocks is less clear.

Brittle veins related to multiple metasomatic stages are ubiquitous across the E1 Group mine lease. Early albite and pre-ore K-feldspar veins are common, but are generally small (< 10 cm) and volumetrically less significant than later stages. Pre-ore magnetite and biotite veins are typically less than 1 cm thick, although the boundary between magnetite veins and magnetite alteration is usually impossible to distinguish. Indeed, much of the magnetite is characterized by massive texture and cannot be linked to obvious conduits at sub-meter scales. Albite, K-feldspar, hematite and biotite veins are generally absent in the discordant breccia, though it is extensively altered by these same minerals. Ore-stage carbonate veins are found throughout the mine lease and extend beyond drilling; they are volumetrically the dominant vein type. Within and proximal to the ore zone, the veins also host barite, fluorite, chalcopyrite, and pyrite. The veins are abundant in the brittle metavolcanic rocks and discordant breccia, but are relatively less common in the metasedimentary rocks and strongly-foliated rocks. Carbonate vein thickness ranges from sub-millimeter to > 5 m. The carbonate veins typically form conjugate sets and the orientation of carbonate veins is shown in Figure 17d. These veins are typically subvertical and some of the larger veins (up to 1 m thick) appear to be linked to Faults 1 and 3 in E1 North (Fig. 14). However, the veins frequently

reopen earlier feldspar, magnetite and biotite veins and metamorphic fabrics resulting in variable orientations. Some microveins, defined herein as having widths less than 5 mm, follow bedding and are difficult to distinguish from layer-parallel alteration when obscured by sulfide selvages. Overall, alteration in the system is dominated by replacement of primary bedding or shear layering and veins are not a major host to mineralization.

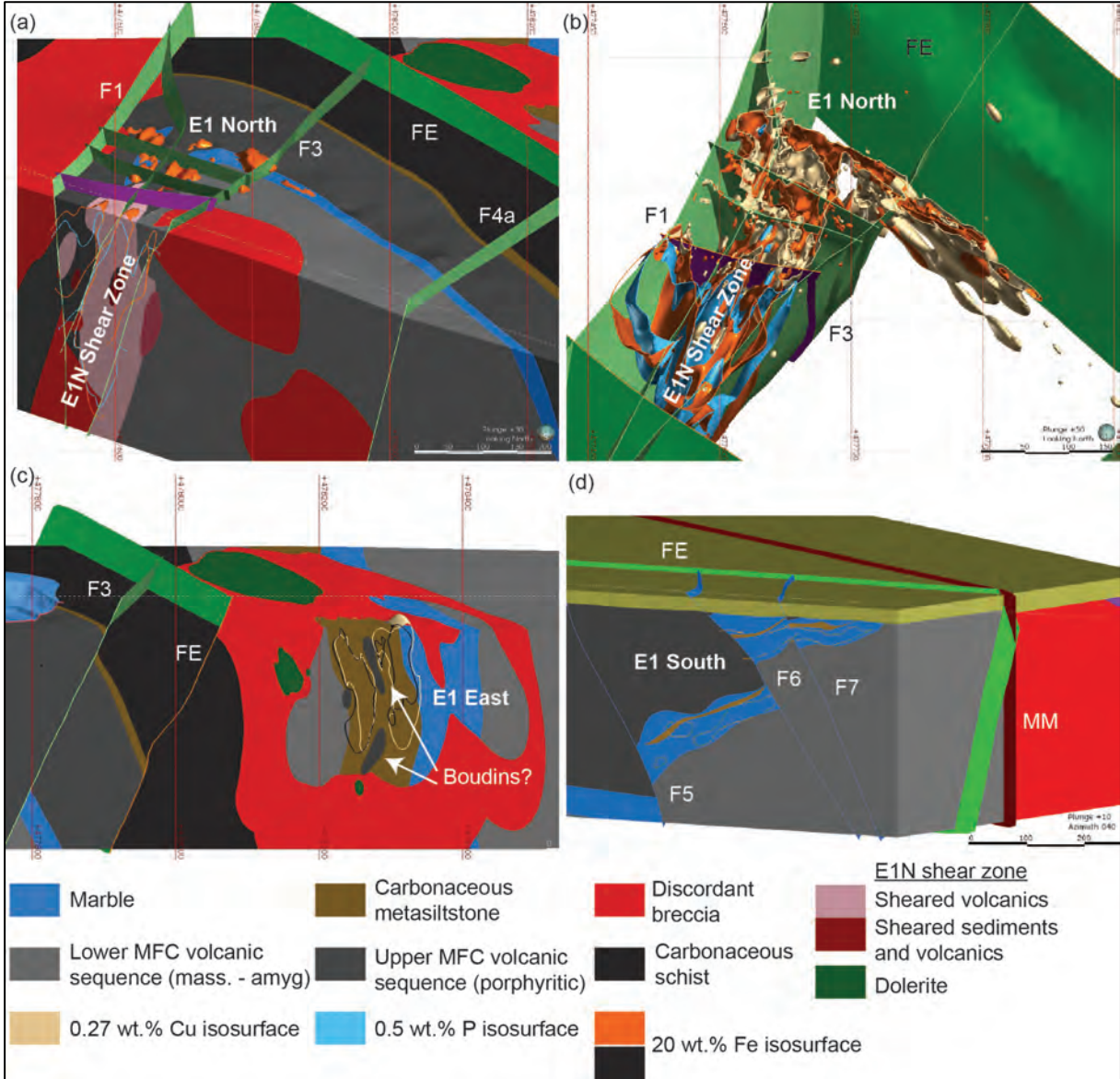


Figure 15: Deposit-scale structures of the E1 Group. (a) E1 North Shear Zone and associated Fe-P (magnetite-apatite) alteration zones. (b) Horizontal slice showing zonation along E1 North Shear Zone from Cu orebody to Fe-P zone. (c) Slice through E1 East orebody showing boudinaged? porphyritic metavolcanic rocks within the metasiltstone ore lens. (d) Slice, looking 040, through E1 South showing offset of Cu-Fe mineralization by D₄ Faults 5-7. Note that Cu concentrations are higher below the metatuff lens.

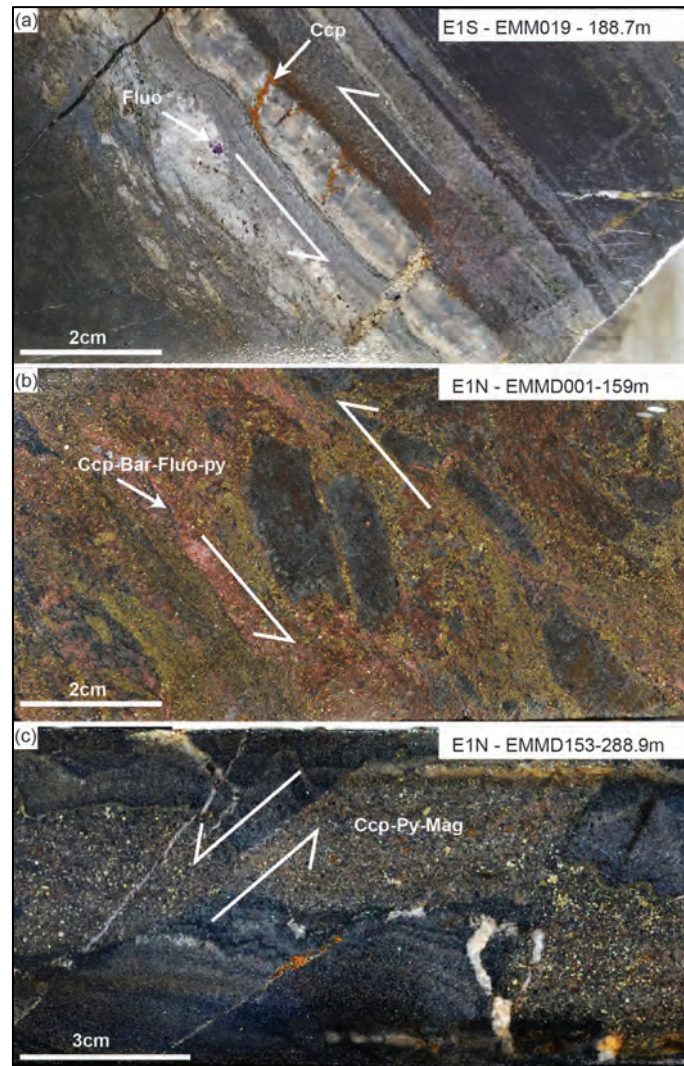


Figure 16: Small-scale structures. (a) Boudinage of silica-rich layers in siliceous marble. Note carbonate-fluorite-pyrite-chalcopyrite veins forming boudin necks. (b) Sheared metavolcanic breccia? or siliceous metasedimentary rock. Groundmass is entirely pyrite-magnetite-chalcopyrite-barite-albite-fluorite-altered. (c) Dilation in magnetite-altered marble with magnetite-pyrite-chalcopyrite infill, associated with sinistral faulting and shearing? Ccp, chalcopyrite; Mag, magnetite; Bar, barite; Fluo, fluorite; Py, pyrite.

Deformation sequence

The deformation events presented in this section refer to local events in the E1 area, except in instances where a regional correlation is explicitly made. Correlations between E1 and regional deformation are discussed later.

D₁ and D₂ and earlier deformation events

The earliest deformation in the E1 Group area is represented by foliation sub-parallel to compositional layering preserved in some pelitic metasiltstones (Fig. 18A), and is interpreted as an S₁ fabric formed during local D₁. This fabric is largely obscured by D₂ and D₃ fabrics. The most prominent D₂ structure is the Mount Margaret Fault, which is a first-order, N-S-trending, structure clearly visible in aerial RTP-TMI over 20 km north and south of the E1

Group (Fig. 9). It is the only structure in the vicinity of the E1 Group that clearly offsets the Mesozoic cover. Blenkinsop *et al.* (Fig. 10a; 2008) implied that the Mount Margaret Fault represents a northern extension of the regional Cloncurry Fault structure, which probably originated as a syn-depositional basin-bounding normal fault and was subsequently reactivated as a major thrust during regional D_2 and later episodes of the Isan Orogeny (Austin and Blenkinsop 2008; Blenkinsop *et al.* 2008; Austin and Blenkinsop 2010). D_2 also formed the S_2 foliation which is dominant throughout the E1 Group area. S_2 foliation is defined by mica cleavage in pelites as well as flattening and alignment of metavolcanic breccia clasts and amygdules (Fig. 18B). Fine-grained ($< 100 \mu\text{m}$), highly-deformed quartz veins, up to 1-2 cm thick, are present in some schists and are folded into alignment with S_2 , and are interpreted to represent pre- to syn-metamorphic veining. S_2 trends N-NW and dips steeply W (Fig. 17A), and is typically parallel to axial surfaces of parasitic macrofolds observed in drill core (Fig. 18D). Although amygdules are generally foliated, primary flow textures are preserved in most plagioclase-rich metavolcanic rocks, implying that they did not absorb substantial penetrative strain during D_2 . Development of S_2 foliation was concurrent with formation of the deposit-scale folds (Figs. 11, 17C), which were caused by east-northeast—west-southwest shortening. The orientation of S_2 and the folds are similar to D_3 fabric reported by Rubenach *et al.* (2008); however, this event did not produce major folding in the Eastern Fold Belt and D_2 structures at the E1 Group most likely correspond to regional D_2 and peak metamorphism.

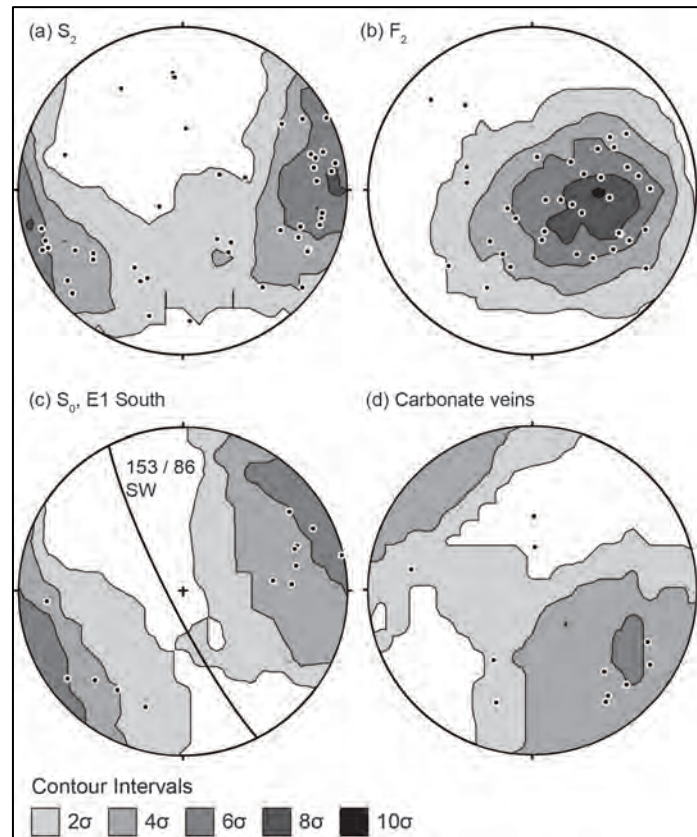


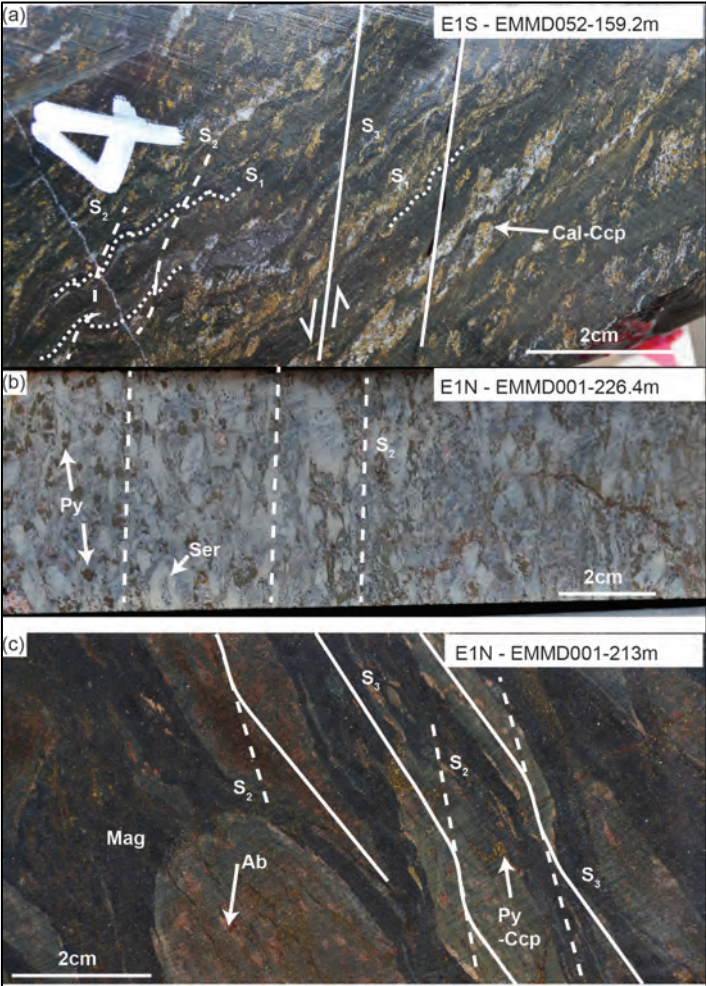
Figure 17: Poles of drill core structures plotted on equal-area southern hemisphere projection. Contours based on the Kamb (1959) method. (a) S_2 fabric associated with D_2 , generally axial planar to F_2 folds. (b) F_2 fold axes. (c) Bedding from both limbs of the E1 South synform and calculated axial plane of the synform. (d) Orientations of carbonate veins.

D₃ deformation event

The E1 North Shear Zone and bounding faults represent a brittle-ductile D_3 structure which crosscuts the E1 North Antiform formed during D_2 . Ore-stage calcite veins exposed in the E1 North open pit near Fault 3 are mostly subvertical and dip southeast (Fig. 14B), though some of the larger veins (up to 1 m thick), observed in drill core and modeled, dip $\sim 60^\circ$. Other large veins form perpendicular to Fault 2 and dip $\sim 45^\circ$ west southwest (Fig. 11D). These orientations indicate normal sense movement under locally-extensional stress regimes, and the veins are interpreted to represent extension vein structures associated with shear zones and faulting in the E1 North Shear Zone. Asymmetric boudinage is common throughout metasedimentary rocks in the E1 Group and is consistent with extensional regimes. The extensional movement of the E1 North Shear Zone and related faults can be explained by accommodation of dextral movement of Faults E and A in response to dextral movement along Fault 1 and the Mount Margaret Fault caused by northeast-southwest shortening. S_2 foliation is crenulated by S_3 fabric (Fig. 18). Within the E1 North Shear Zone, S_2 is sheared

and locally completely overprinted by S_3 shear fabric (Fig. 18). E1 East metasedimentary rocks are also strongly sheared but the kinematics in this area are not constrained, though Cu concentration shell distributions suggest that shearing was parallel to the northwest-southeast trend of the E1 East Antiform in which the orebody is hosted (Fig. 19a).

Unlike the strongly-foliated metavolcanic breccias, the discordant feldspar altered breccias crosscutting the system are generally only locally deformed and contain clasts of porphyroblastic metasedimentary rocks, indicating that this breccia formed after D_2 . Weak foliation is developed in the biotite-rich matrix of the discordant breccia, and clasts are locally strongly foliated. The contact of the breccia with intact wall rock is strongly sheared at E1 North, and thus it is likely that brecciation occurred after D_2 and prior to or during D_3 .



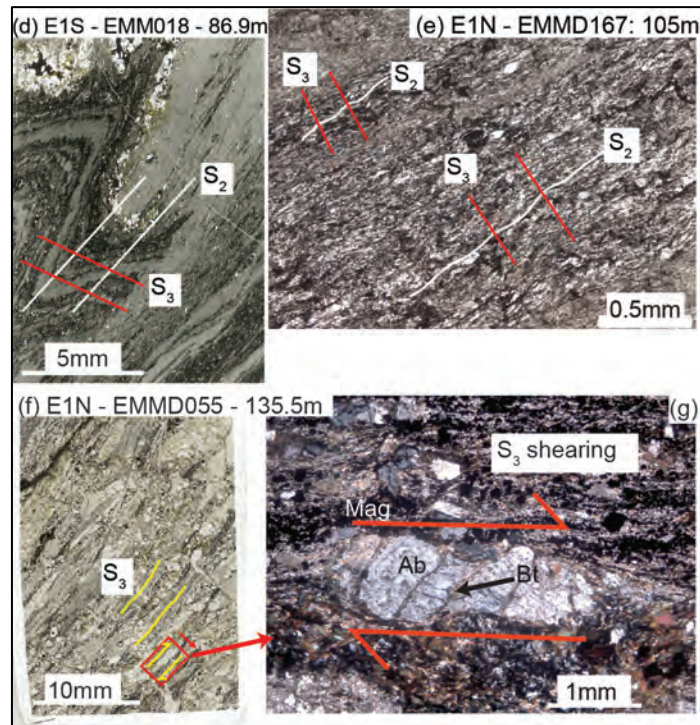


Figure 18: Photomicrographs of representative deformation fabrics. (a) S1 compositional layering in graphitic chlorite metasilstone, crenulated by S₂ and S₃. (b) S₂ flattening of metavolcanic breccia clasts. Note the white haloes in clasts caused by magnetite leaching. (c) S₃ shearing of S₂-foliated metavolcanic breccia or possibly a pseudobreccia. Groundmass is mostly magnetite with blebby sulphides. Note phenocrysts in “clasts”. It is unclear if the magnetite is replacing an S₃ shear fabric forming a pseudobreccia in porphyritic metavolcanics, or if the magnetite is replacing primary breccia matrix. (d) and (e) S₂ fabric in carbonaceous schist axial planar to folding, crenulated by S₃. (f) S₃ shearing of plagioclase-phyrlic metaandesite. (g) photomicrograph of area noted in (f), showing dextrally-sheared albitized plagioclase phenocrysts; cross polarized light. Pre-ore biotite veins antithetic to the shear suggest syn-shearing timing. Opaque mineral is pre-ore magnetite.

D₄ and later deformation events

The northeast-trending faults bounding the E1 North Shear Zone were reactivated in oblique-slip movement with dominantly a reverse-slip component during D₄. Faults 4-7 formed at this time with similar orientations, and also experienced both reverse and sinistral or dextral movement (Fig. 11). The reactivation of these faults suggests shortening was approximately south-southeast to north-northwest. Offset of Fault 4 by Fault E suggests that the latter was also reactivated following D₄. The D₄ faults offset alteration and post-date mineralization, though some zones of supergene enrichment in Co and Mo are clearly associated with these structures (see next section; Fig. 19). Strike-slip movement along Faults 1 and 2 is minimal as they do not laterally offset the conjugate shear zones or mineralization. Offset of the Mesozoic sediments by 10–20 m at the Mount Margaret Fault indicates that this structure was reactivated up to the Mesozoic.

3-D concentration distribution modeling

Datasets

Geochemical modeling interpolations of the Cu, Au, Fe, S, P, Co, Mo, U and La concentration shells presented in this study are based on assay data provided by the current mine operator, which consists of a pre-open pit DDH and RC (Reverse Circulation) multi-element suite including all of the aforementioned elements, as well as a dataset from blast hole sampling for E1 North open pit which includes Cu, Au, Fe, S, and Co. The assays were prepared by triple-acid (HCl, HNO₃, and HClO₄) digestion and analyzed via inductively-coupled plasma atomic emission spectroscopy (ICP-AES) for Au and trace elements at ALS Laboratories in Townsville, Australia. Copper was analyzed by inductively-coupled plasma atomic absorption spectrometry (ICP-AAS). Assay interval lengths generally vary between 1 m and 2 m for DDH and RC samples, and many visually unmineralized intervals were not sampled. Blast hole samples represent homogenized averages of the entire hole length, which varies from 8 m to over 20 m. While down-hole sample resolution is lower in the blast holes compared to the DDH and RC holes, the former are spaced < 5 m in all directions and provide much higher spatial resolution in the E1 North orebody. Phosphorus, U and La were not analysed in blast hole samples, but a comparison of Cu interpolants incorporating and excluding blast hole data demonstrates that major structures can still be resolved with only DDH and RC drilling, and meaningful interpretations can be made. Below-detection values are not listed in the database and could not be distinguished from unsampled intervals. For this reason, below-detection values were not replaced and all missing values were omitted from interpolation. Summary statistics of the assay data are available in Appendix 2. Energy-Dispersive Spectroscopy (EDS) was conducted on a JEOL JXA-8200 Superprobe at the James Cook University Advanced Analytical Centre to help identify the host minerals of the modeled elements.

Concentration interpolation parameters for the E1 Group

Numerical implicit modeling of geochemical assay data was conducted using the Multi-domained Interpolation function. Leapfrog uses fast-Radial Basis Functions (RBF) for implicit modeling, as described in detail in Stewart *et al.* (2014). The output of fast-RBFs is comparable to ordinary and dual kriging (Stewart *et al.* 2014). Table 1 displays the interpolation parameters used for all elements in this study. In addition to these parameters, a structural anisotropic trend was applied to each interpolant to reflect the stratabound morphology of the orebody. The orientation of the trend is derived directly from the

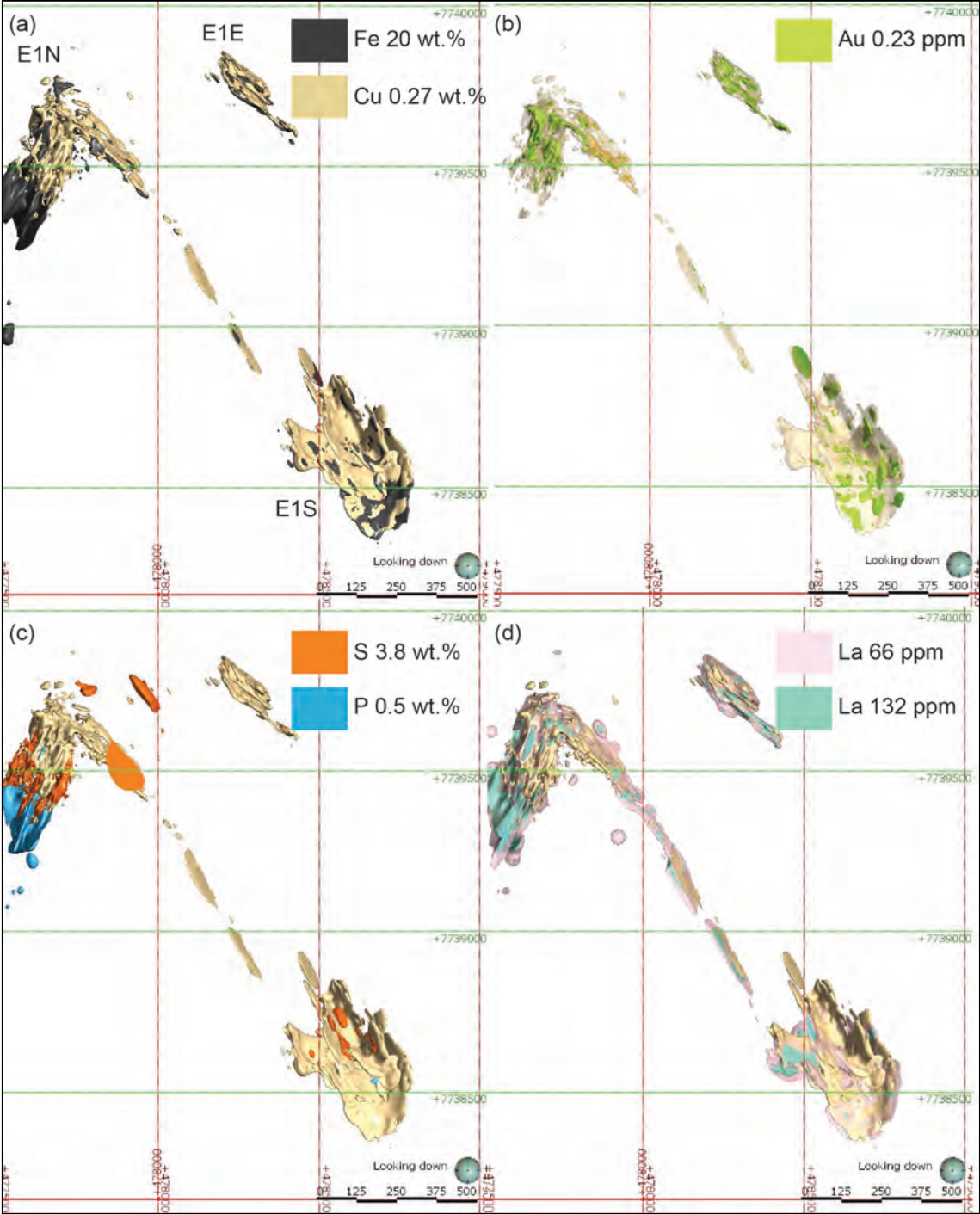
combination of meshes of the modeled metasedimentary rock units that host the ores, as well as from meshes of the mineralized D₃ structures observed at E1 North. Isosurfaces of the output interpolants are presented in Figure 19.

Isosurface values for copper and gold were selected as the cutoff values between economic and sub-economic concentrations used by the mining company. These cutoffs are probably orders of magnitude higher than thresholds between regional background and anomalies, but they have been chosen because the elements are of economic interest. Cutoff values for copper and gold are 0.27 wt.% and 0.23 g/t, respectively. Cobalt, Mo, U and La follow approximately log-normal distributions (Appendix 1) and are characterized by < 10% outliers, enabling anomalous isosurfaces to be calculated using the median + 2MAD (median absolute deviation) method (Reimann 2005). This yields anomalous lower thresholds at 74 ppm, 25 ppm, 23 ppm and 66 ppm, respectively. Thresholds of these elements calculated using the box plot inner fence method (Tukey 1977) were around an order of magnitude (e.g. Co 300 ppm) higher than their average crustal abundances and, at best, represent maximum background cutoffs. The lower thresholds determined from the median + 2MAD method are preferred. Iron, S, P do not follow normal or log-normal distributions and their lowest isosurface values were arbitrarily set to their mean concentrations in ore-concentration (> 0.27 wt.% Cu) zones (17 wt.% Fe, 2000 ppm P, 2.8 wt.% S).

Interpolation results

Structurally-trended concentration isosurfaces of Cu, Au, Fe, S, P, Co, Mo, U and La are presented in Figure 19. Cobalt, Mo, and U (Fig. 19e-g) coincide with the Cu-Au orebody (Fig. 19a-b), while Fe, P, La and S (Fig. 19a, c-d) overlap but show significant zonation from northeast to southwest away from the ore zone. The Fe, Cu and S interpolants (Fig. 19a, c) strongly coincide with E1 North Shear Zone structures. Although the resolution of the P assay is lower, it is high enough to resolve association with the E1 North Shear Zone southwest of the orebody. All elements are enriched within the Corella marble horizon extending from E1 North to E1 South. The Co anomaly (≥ 74 ppm; Fig. 19e) extends beyond mineralization for up to 20 m in the more stratibound zones of the orebody, but extends along strike of the E1 North Shear Zone for over 150 m. Anomalous La and U (> 66 ppm and > 23 ppm, respectively) are modeled up to 250 m and 180 m respectively along the shear zone, and are restricted to 20–40 m outside the Cu orebody at E1 East and South (Fig. 19d, g). The Mo

anomaly (> 25 ppm; Fig. 19f) is present up to 50 m outside mineralization at E1 North, but is restricted to < 20 m elsewhere in the E1 Group.



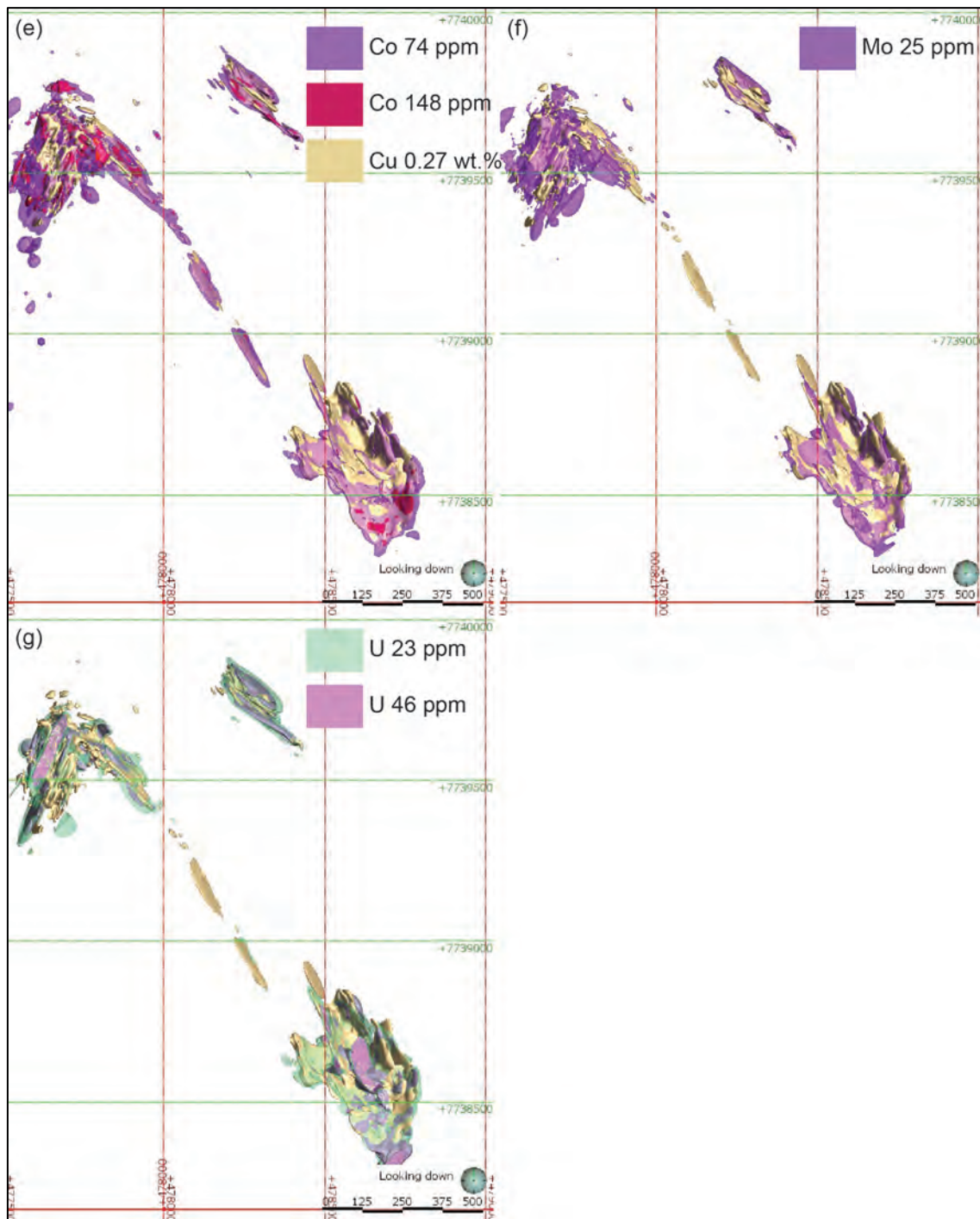


Figure 19: Plan view of isosurfaces of structurally-trended interpolants. Note the higher resolution at E1 North for Cu, Fe, S, and Mo as a result of additional blast hole data. Copper and gold isosurface values are based on mining cutoff concentrations, while S, P, and Fe are based on the mean concentrations of these elements in ores. Isosurface values for La, Co, Mo and U are based on anomalous cutoffs determined using the median + 2MAD (median absolute deviation) method (Reimann, 2005).

(a) Cu and Fe isosurfaces. (b) Cu-Au. (c) S and P. (d) La isosurfaces at anomalous and 2X anomalous values. (e) Co isosurfaces at anomalous and 2X anomalous values. (f) Mo. (g) U isosurfaces at anomalous and 2X anomalous values. Blowouts in S, Co, Mo, U are artificial and extend into the unaltered cover sediments. This is caused by the interpolation models having the same extents as the geological model in which they are subdomained. Leapfrog cannot clip the interpolants to a particular surface or volume.

Interpretations

Drill core, petrographic, and EDS observations enable the modeled element distributions to be linked to specific alteration phases. Drill core logging indicates that the interpolated high-S

zone corresponds to pyrite alteration, while the Fe-P-rich zone is characterized by widespread coarse-grained, euhedral magnetite-apatite \pm pyrite replacement. Energy-dispersive spectroscopic analysis demonstrates that the high La anomaly is hosted within apatite and trace monazite. In the ore zone there is less apatite and REE alteration is also contained in bastnäsite and monazite. Uranium and S are enriched to over 200 ppm and 10 wt%, respectively, in the carbonaceous metapelite at E1 South. Such high S content is attributable to the *c.* 5 vol.% pyrite content of this rock, which may be diagenetic in origin but has since been recrystallized. Uranium is naturally high in carbonaceous metasedimentary rocks (Vine and Tourtelot 1970), which may explain the elevated values. Enrichment of Co, Mo and U near the basement-cover unconformity is likely due to supergene remobilization. These elements are also anomalous at the surface above 30–50 m of thick cover (Lilly *et al.* 2013). Molybdenite is rare in the deposit, and Mo and Co-rich phases have not been observed in EDS analysis, suggesting that they are hosted within another phase.

Discussion

Relative timing of alteration and mineralization

At the deposit scale, interpolated Cu and Fe element concentration shells form clear lineaments associated with the E1 North Shear Zone and conjugate shear zones B-D, indicating that these local D₃ structures were active during mineralization (Figs. 14, 19). This is consistent with microscale observations of pre-ore biotite veins crosscutting antithetically to dextrally-sheared, albitized, plagioclase phenocrysts (Fig. 15g), which indicates a pre-syn local D₃ shearing timing for early albite alteration, and syn-shearing timing for pre-ore potassic-ferric alteration. Furthermore, hematite alteration associated with early albite is aligned to the shear fabric (Fig. 18g), which is also consistent with a pre to syn-shearing timing. Pre-ore quartz associated with magnetite is locally deformed at grain boundaries and provides further evidence of on-going deformation during mineralization. Faults 4 to 7 are not associated with alteration and actually offset it, indicating that local D₄ took place after mineralization. Additionally, a lack of abundant horizontal veining associated with Faults 1–3 suggests that the reverse movement on these structures during D₄ was not associated with any substantial hydrothermal activity and alteration.

Structural controls on mineralization in the E1 Group

Structural permeability in the E1 Group is provided mainly by fold hinges and shear zones. Mineralization is focused at/near the hinges of the E1 North Antiform and E1 South Synform, and the paucity of major mineralized structures at E1 South suggests that dilation in the synform hinge itself acted as a major fluid focusing zone during mineralization. This is in agreement with the presence of smaller-scale dilations in the hinges of <1m parasitic folds at E1 South. These dilations focus hydrothermal carbonate, quartz and pyrite. The bounding of the E1 metasedimentary rock horizons by relatively impermeable metavolcanic rocks may have enhanced focusing of fluids into these dilational zones. Intersection of the E1 North Antiform, in particular the marble horizon that defines it, with the E1 North Shear Zone (Fig. 15) is the most likely explanation for higher ore concentration and tonnage at E1 North compared to East and South. It is also possible that the E1 North antiform experienced more dilation than E1 South, but this does not explain the extent of alteration along strike of the southwest limb. The E1 North Shear Zone focuses alteration along strike, nearly parallel to the limb of the antiform, for more than 1 km. Alteration along the shear zone changes from the apatite±magnetite zone in the southwest, to the magnetite zone, pyrite zone, and finally the magnetite-barite-fluorite-carbonate-chalcopyrite ore zone near the hinge of the E1 North Antiform. The orientation of the shear zone appears to be mostly controlled by the west limb of the antiform. It is possible that strain partitioning along this shear zone may have been enhanced by the discordant breccia body that is partially fault-bound to the west by Fault 1 (Fig. 11). This breccia is relatively undeformed compared to the adjacent strongly-sheared metavolcanic breccias and metasedimentary rocks in the E1 North Shear Zone. The breccia also shows strong albite-K-feldspar-alteration, which may have strengthened the breccia and inhibited shearing except at localized high-strain zones < 5 m wide.

The northeast-southwest trending shear zones at E1 North are not recognized at E1 East. Interpolation of Cu concentration suggests that the orebody trends in the same direction as the host limb of the E1 East Antiform. However, it is notable that the E1 East ore zone occurs adjacent to the onset of major curvature in this antiform. Shear parallel to layering is abundant in drill core and probably acted as the major fluid conduit at E1 East. The contact between metasedimentary and metavolcanic rocks, regardless of stratigraphic conformity, is not a significant control on mineralization at the deposit scale, as high ore concentrations (> 1 wt.% Cu) are typically found over 5-10m away from contacts at E1 South (Fig. 15c).

At the deposit scale, the concentration interpolation models suggest that ores not directly associated with a specific structure are restricted mostly to the Corella metasedimentary rocks. This may suggest that metasedimentary composition and bedding are major mineralization controls. The chemical favourability for carbonate rocks for sulfide alteration is well-documented in skarns (Meinert, 1992). Evidence of these controls at smaller scales can be observed in preferential alteration along beds, including flaser crossbedding. Although bedding contacts are not a major control at the deposit scale, lamination-parallel microveining (< 5 mm width) is common and may have acted as a major fluid pathway. These microveins are difficult to distinguish from coarse-grained (> 2 mm) alteration without petrographic analysis. It is possible that the microveins open along bedding sub-parallel S_1 , and that S_1 itself has enhanced bedding permeability. Locally, high ore concentrations are carried by thick (> 30 cm) carbonate veins that typically reopen earlier veins of quartz, albite and K-feldspar. The carbonate veining and localized brecciation is more abundant in the more competent coherent metavolcanic rocks, but these veins and breccias are only slightly mineralized. Disseminated carbonate alteration haloes are associated with some carbonate veins, but at the drill core scale these haloes are only sporadically associated with strong magnetite-chalcopyrite alteration. It may be that these larger veins were either not a major conduit for mineralization, or that the system at that time was characterized by relatively low water-rock ratios. Boudin necks and microfaults within the metasedimentary rocks focus alteration and are typically infilled by carbonate, chalcopyrite and pyrite veining with wide (c. 1 cm) chalcopyrite-pyrite selvages.

Timing of IOCG mineralization in Cloncurry

Understanding the relative timing of mineralization with respect to formation of structural conduits is critical for improving IOCG genetic models. At the Ernest Henry deposit, mineralization is interpreted to have taken place after peak metamorphism (D_2) and during both local and regional D_3 (Twyerould 1997; Coward 2001; Mark *et al.* 2006). These relationships are consistent with the E1 Group orebody having formed during local D_3 . At the present, no reliable ages are available for the E1 Group; however, Ernest Henry alteration has been dated via Re-Os (molybdenite) by Mark *et al.* (2004) and via U-Pb (titanite) by Mark *et al.* (2006). These data are shown in Figure 4, together with correlations between the E1 Group and Ernest Henry and regional deformation histories. Both dating methods constrain the timing of ore genesis at Ernest Henry to 1530-1500 Ma. .

Ernest Henry and the E1 Group share local D₃ mineralization timing and regional D₃ kinematics. However, the absolute age of Ernest Henry is closer to regional D₄ (Figs. 3-4). Although no reliable U-Pb or Re-Os ages have been obtained for the E1 Group and Monakoff mineralization, Williams *et al.* (2014) indicate that they are probably related to the Malakoff Granite, which forms part of the 1530–1500 Ma Williams-Naraku suite and overlaps in time with Ernest Henry. The discrepancy between the relative and absolute timing of these deposits with respect to regional D₃ and D₄ could be explained in two ways.

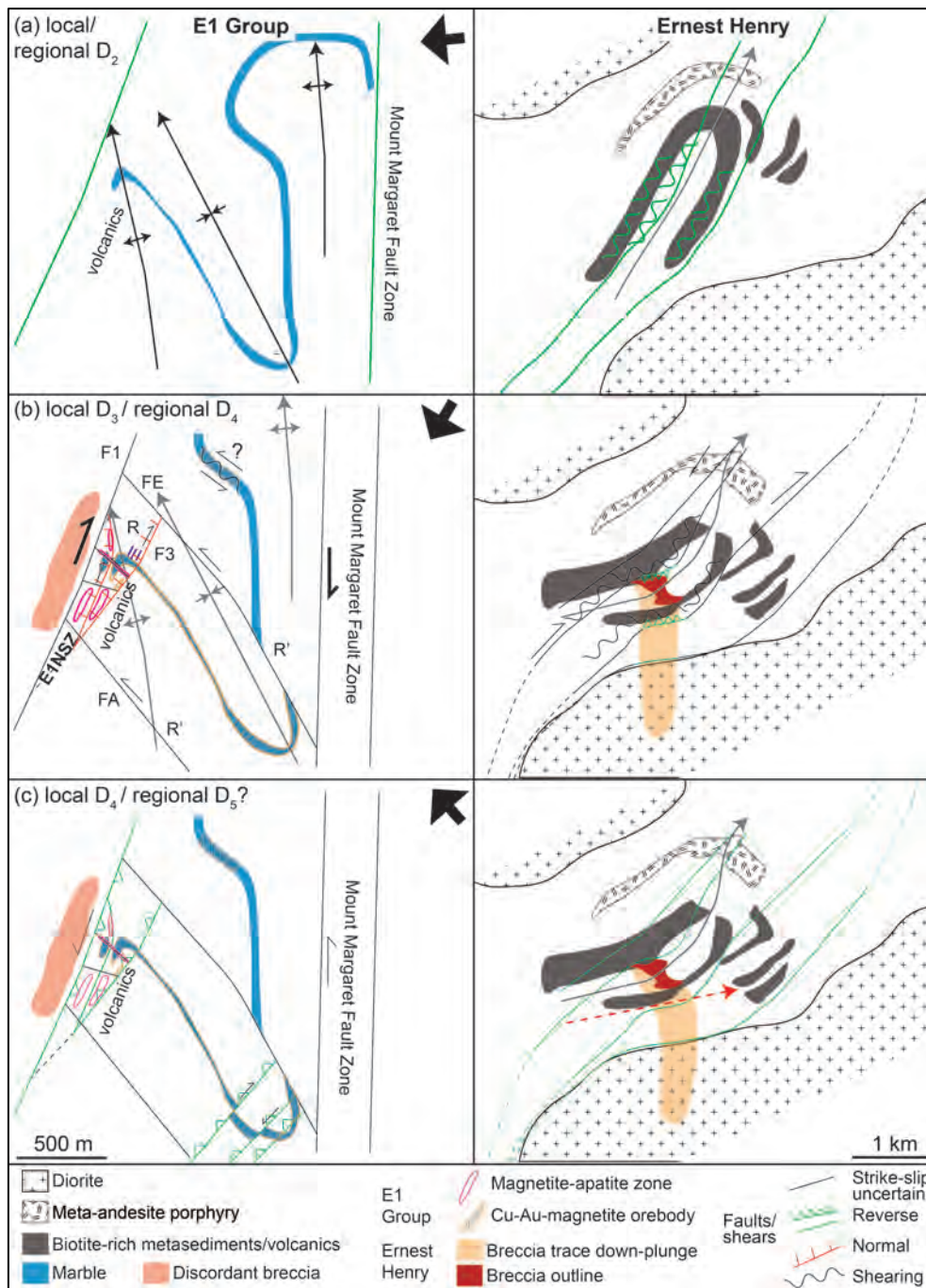


Figure 20: Conceptual model of the structural history of the E1 Group and Ernest Henry deposits. (a) Regional D_2 folding generates pre-mineralization tectonic fabric. At E1, Fault 1 and Mount Margaret faults probably activated as thrusts during this time. At Ernest Henry, sedimentary rocks are folded around Ernest Henry Diorite, and the orebody-bounding shear zones, possibly parallel to existing sediment layers, are initiated. (b) In local D_3 / regional D_4 , the shortening direction (indicated by the black arrows) shifts northward causing dextral reactivation of D_2 faults at E1. Sinistral northwest-trending faults are formed, and E1 North shear zone develops as probably normal-dextral conjugate structures, with shear zones mainly focused along the marble horizon between more competent breccia and volcanic rocks. At Ernest Henry, D_2 shear zones reactivated in a reverse flower structure in response to probably dextral shearing along the main shear zone around the competent diorite bodies. During this time, mineralization takes place in both systems. At Ernest Henry, competent volcanics between sheared metasediments deform in a brittle manner and brecciate with sufficient fluid overpressure. At E1, strain is mostly focused in the metasediments and volcanic breccias. (c) After local D_3 , northwest-southeast-directed shortening (local D_4) causes reverse faulting at E1, and northeast-southwest-oriented gentle folding of the Ernest Henry orebody.

First, regional D₃ may not be focused significantly in the E1 Group-Ernest Henry area. Variability in the intensity of regional D₃ and D₄ fabrics and structures have been documented by other authors (e.g. Rubenach & Barker 1998; Austin & Blenkinsop 2010; Duncan *et al.* 2014), especially in the vicinity of the Cloncurry Fault (Austin & Blenkinsop 2010). Second, it is possible that the direction of shortening in regional D₄ is heterogeneous over the distance between the Snake Creek Anticline and the E1 Group. Such heterogeneity has been documented across the Mount Isa Inlier by Abu Sharib & Bell (2011), who describe zones of dominantly east-west shortening, north-south shortening, and northeast-southwest shortening. The latter is more localized, especially in the northern part of the Inlier where Ernest Henry and the E1 Group are located. The preferred explanation is a combination thereof, in which regional D₃ strain was not focused in the E1 Group-Ernest Henry region, and the direction of subsequent D₄ shortening shifted from northwest-southeast in the Snake Creek Anticline, to northeast-southwest. Thus, despite being characterized by kinematics similar to regional D₃, the E1 Group probably formed during regional D₄. The post-mineralization, local D₄, structures thus formed in a regional D₅ event which has been recognized by some workers (Fig. 3; Austin and Blenkinsop 2010; Duncan *et al.* 2014). At Ernest Henry evidence for this is observable as late, northeast-trending reverse faults transecting the orebody (Coward 2001), as well as gentle folding of the orebody about an east-northeast-trending hinge (Fig. 20c).

Comparison of the structural controls on the E1 Group and Ernest Henry deposits

The structural setting of the Ernest Henry deposit has been extensively analyzed, and deposit-scale controls on mineralization are well-constrained (Twyerould 1997; Mark *et al.* 2000; Coward 2001; Mark *et al.* 2006). However, camp- and regional-scale controls have not been well-studied in this area due to the paucity of outcrop. Although structural controls in ore deposits are typically complex and somewhat unique to each system, similarities and differences can be found between Ernest Henry and the E1 Group which may help to explain structural factors influencing the style of IOCG mineralization in a given district: i.e., breccia-hosted Ernest Henry-style orebodies compared to shear-replacement E1 Group-style orebodies. In the case of these two deposits, at least four major factors combined to influence their location and mineralization styles throughout their structural evolution: 1) structural ground preparation through D₂ folding and faulting, 2) local normal or reverse faults/shear zones, formed within larger wrench shear systems, enabling dilation and fluid influx, 3) strain partitioning caused by rheological contrast between volcanic and sedimentary protoliths and, 4) fluid overpressuring.

The major folds hosting Ernest Henry and the E1 Group were developed prior to mineralization. The hanging wall and footwall shear zones that bound the Ernest Henry orebody are splay structures related to a larger, northeast-trending, brittle to ductile zone that developed in east-west shortening during regional D₂. The shear zones provided the structural framework for later syn-mineralization deformation (Twyerould 1997; Coward 2001). The northeast-trending orientation of these shear zones, along with the possible fold hinge they form around, are not consistent with north-northwest D₂ fabrics. This suggests that they may have been rotated during local D₃ (Fig. 20c). At the E1 Group, D₂ formed the north-northwest plunging E1 North Antiform with its western limb trending northeast-southwest.

During local D₃ / regional D₄, the D₂ structures in both deposits were reactivated with components of dip- and strike-slip movement, leading to dilation that could focus mineralizing fluids (Fig. 20). In the E1 Group, the north-northeast-trending Fault 1 and Mount Margaret Fault structures probably experienced dextral and reverse slip in response to northeast-southwest shortening, resulting in formation of a transpressional Riedel brittle to ductile system (Cloos 1928; Riedel 1929; Davis *et al.* 2000) (Fig. 20b-c). Less competent sedimentary and volcanoclastic rocks experienced shearing associated with this faulting. Faults A and E may have formed as sinistral antithetic R' brittle to ductile zones to this wrench system, while the E1 North Shear Zone and associated conjugate structures may have formed as synthetic R brittle to ductile zones. The orientations of Faults A and E are northwest-trending, rather than southwest (in an ideal Riedel system). This is probably caused by utilization of the existing north-northwest trend of the major folds. Because of the pre-existing northeast trend of the west limb of the E1 North Antiform, the E1 North Shear Zone developed as both a R brittle to ductile zone and normal structure to accommodate northwest-southeast directed extension. At Ernest Henry, the northeast-southwest shortening associated with D₄ formed a series of moderately-dipping, reverse shear zones between the diorite bodies at Ernest Henry, resulting in dilation. In contrast to the E1 Group, the dilation caused brecciation of metavolcanic rocks by the Cu-Au-bearing fluids (Twyerould 1997; Coward 2001; Mark *et al.* 2006). Overall, the E1 Group and Ernest Henry deposits record the same sequence of deformation events from at least D₂ onward. However, the mineralizing event in D₄ resulted in contrasting orebody styles: hydrothermal breccia ores at Ernest Henry, and replacement ores at the E1 Group.

Protolith competency contrasts Cover Sequence 2 may have helped to focus the D₄ structures that host the Ernest Henry and the E1 Group deposits. In this part of the Eastern Fold Belt, Cover Sequence 2 is made up mostly of intercalations of the competent Mount Fort Constantine Volcanics and more ductile Corella Formation metasedimentary rocks. Cross sections of Ernest Henry (e.g. Twyerould 1997; Coward 2001) reveal marble and metasilstone rock horizons in the footwall sequence immediately underlying the ore breccia zone. The horizons are coincident with the shear zones that bound the orebody. These metasedimentary rocks are generally characterized by strong biotite and carbonate shear foliation; more silica-rich beds are boudinaged and brecciated (Twyerould 1997). Marshall & Oliver (2008) suggested that this intercalation of metavolcanic rocks and Corella marble resulted in brittle strain developing in the former concurrently with ductile strain focusing in the latter.

The footwall metasedimentary rocks at Ernest Henry are comparable to those at the E1 Group, which suggests that these shear zones are likely controlled by the original stratigraphic position of the sedimentary and volcanic rocks. In both cases, D₄ shear strain was mostly partitioned into the ductile Corella Marble and other metasedimentary horizons between more competent coherent metavolcanic rocks and metasilstones. Strain partitioning was facilitated in each system by the pre-existing northeast-southwest orientation of the sedimentary and volcanic rocks resulting from the D₂ folding. Although metasedimentary rocks focused most of the ductile strain in both deposits, these rocks are not mineralized at Ernest Henry. It is possible that juxtaposition of competent volcanic rocks (Fig. 5b) between the sedimentary rocks increased the amount of brittle strain focused into the former, leading to brecciation. This is in contrast to the E1 Group, where the volcanic rocks surround the sedimentary rocks, causing much less strain to develop in the volcanic rocks.

Relative fluid overpressure (where fluid pressure > lithostatic pressure) may also help explain the contrasting mineralization styles between the E1 Group and Ernest Henry. These parameters, in addition to the fertility of the source fluid(s), may account for the higher tonnage and concentration of the latter. Oliver *et al.* (2006) demonstrated that the process of rapid, fluidized brecciation by potentially mineralizing fluids could explain the breccia textures observed at Ernest Henry and other, barren hydrothermal breccias in the region. Marshall & Oliver (2008) implied that this process may have taken place at Ernest Henry, in part due to overpressuring by an impermeable footwall marble layer. However, the

replacement of sheared marble and other metasedimentary rocks in the E1 Group provide clear evidence that marble can also preferentially act as a sink of ore fluid metasomatism rather than a barrier.

It is likely that brecciation or replacement can take place depending on the relative permeability of the volcanic and metasedimentary rocks. This is governed by the partitioning of strain, as previously discussed, as well as by the degree of fluid overpressure. If strain rate is relatively low, the sedimentary rocks can accommodate most shear strain while the volcanic rocks remain mostly intact and relatively impermeable. However, if strain rate is high, or more strain is focused into the competent rocks, they may fracture and become relatively more permeable than the sedimentary rocks. If fluid pressure is also low enough, micropermeability within the shear zone will be sufficient enough to accommodate hydrothermal fluids, albeit with some fracturing and faulting. The volcanic rocks are less resistant to tension than the sedimentary rocks, and may consequently accommodate most of the strain caused by overpressure (e.g. Gessner *et al.* 2006; Gessner 2009).

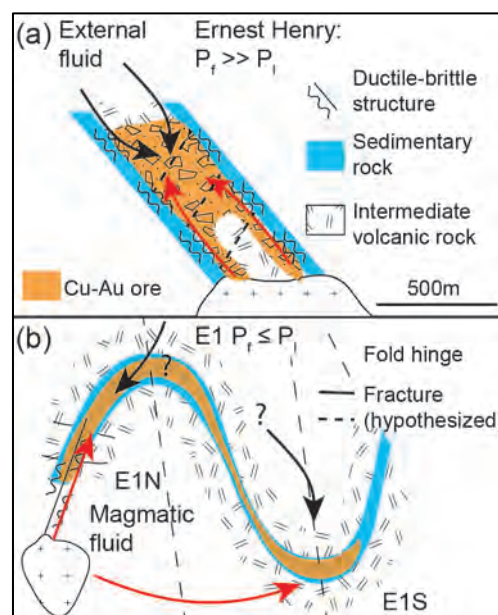


Figure 21: Cartoon of fluid and structural models for Ernest Henry and E1 Group mineralization. (a) At Ernest Henry, a combination of fluid pressures significantly higher than lithostatic pressure, and positioning of competent metavolcanic rocks between impermeable, ductile, metasedimentary rocks (mostly marble) leads to overpressuring of a magmatic-hydrothermal fluid and brecciation of the competent metavolcanic rocks. During this brecciation, an external fluid mixes with the magmatic fluid. (b) At the E1 Group, the ductile metasedimentary rocks, bounded by brittle metavolcanic rocks, focus shearing and hydrothermal fluids, which are under comparatively less pressure (fluid pressure \leq lithostatic pressure).

The degree of fluid overpressure in either system may be related to the overall size and H₂O content of the granitic intrusion that probably contributed to the mineralizing fluids in both Ernest Henry (Twyerould 1997; Mark *et al.* 2006; Kendrick *et al.* 2007; Oliver *et al.* 2008)

and the E1 Group (Williams *et al.* 2014). The P-T conditions at the time of fluid exsolution from the magma, along with the availability of ligands, Cl, and S for transporting and precipitating Cu and Au, are also important. Indeed, models for IOCG genesis in the region (e.g. Mark *et al.* 2006; Kendrick *et al.* 2007; Williams *et al.* 2014) invoke the mixing of a magmatic fluid with another fluid (i.e. basinal or meteoric; Fig. 21), which may have carried much of the necessary sulfur, in order to generate Ernest Henry ore. The size of the E1 Group may be partly dependent on the degree of mixing between such fluids; brecciation may serve as an efficient mixing mechanism. However, the similar mineralogy and chemistry of the two deposits suggests that their fluid characteristics were comparable during mineralization (e.g. Williams *et al.* 2014). The high tonnage and concentration of Ernest Henry compared to the E1 Group is probably a result of either higher overall permeability generated through brecciation, or derivation from a larger or more fertile fluid and metal source(s). Furthermore, brecciation at Ernest Henry may have facilitated more fluid mixing, resulting in more available metals and/or sulfur. Mineralization at the E1 Group was probably enhanced by the chemically favourable nature of marble for sulfide alteration.

Global comparisons

The E1 Group and deposits in its host district share many structural characteristics with Fe-oxide-Cu-Au deposits in the northern Fennoscandian shield and Carajás districts. Like the Cloncurry District, both regions underwent deformation, metamorphism and magmatism around the time of IOCG formation. Billström *et al.* (2010) provide a thorough summary of the tectonic and structural framework and IOCG deposits of the Fennoscandian shield, on which the following comparisons are based. The Fennoscandian shield and Cloncurry are both typified by protracted tectonic and hydrothermal histories spanning >200 Ma, resulting in a wide array of ore deposit styles. The Fennoscandian shield hosts several IOCG deposits, as well as the type-deposit for the related iron oxide-apatite (IOA) class of deposits:

Kirunavaara. The Fennoscandian shield was dominated by rift tectonics and corresponding deposit types (e.g. syngenetic base metal, VMS and ultramafic intrusion-hosted Ni-Cu-PGE) from about 2500 – 1900 Ma. Following this, a subduction zone formed and collisional tectonics began, and lasted until as late as 1650 Ma. Fe-oxide-Cu-Au and orogenic –Au deposits formed in two episodes of deformation and metamorphism from 1900 – 1870 Ma and from 1810 – 1790 Ma; many IOCGs also formed between these major deformation events. Metamorphic grade varies mainly from greenschist to amphibolite facies, though some areas reached granulite facies. Like the E1 Group and Ernest Henry, many of the Fennoscandian

shield IOCGs, such as Gruvberget, Tjärrojåkka, Rakkurijärvi, and Nautanen, are hosted in intermediate-mafic metavolcanic rocks. Nautanen ores are characterized by replacement textures, while the other deposits are dominated mostly by hydrothermal breccias. In some instances (e.g. Gruvberget) Cu-Au-breccias appear to overprint earlier massive magnetite alteration. All of the deposits are spatially associated with splays of regional structures. The Nautanen deposit is noted for being a type-example of shear zone-hosted ores in the district (Billström *et al.* 2010). The Nautanen deposit is therefore the most analogous orebody in the region to the E1 Group, as it is characterized mostly by replacement ores and ductile structures. However, it is distinct from the E1 Group in that it may have formed prior to or during peak metamorphism (Martinsson and Wanhainen 2004).

The Carajàs district in Brazil hosts world-class IOCG deposits including Salobo and Sossego. These two deposits form part of the group of Archean (~2.5 Ga) Fe-oxide-associated Cu-Au±Mo±Ag±U±REE deposits (Grainger *et al.* 2008). The deposits are hosted mainly in a series of Neoproterozoic (2.75- 2.68 Ga) intermediate-mafic metavolcanic and metasedimentary rocks interpreted to have been laid down in an intracratonic rift basin (Grainger *et al.* 2008), which is analogous to Cloncurry. As with the Cloncurry and Fennoscandian shield, metamorphism in this area reached greenschist to amphibolite facies, with local migmatite formation. The Igarapé Bahia-Alemão, Crisalino and Sossego-Sequerinho deposits are typified by breccia-hosted Fe-oxide-Cu-Au ores, while Salobo—the largest deposit in the district—is dominated by massive replacement magnetite-Cu-Au bodies (Requia *et al.* 2003; Grainger *et al.* 2008). Salobo is characterized by ductile-brittle shear zone controls, whereas the other deposits are mostly associated with brittle structures (Requia *et al.* 2003). Grainger *et al.* (2008) suggested that this may be the result of greater formation depth and metamorphic grade (amphibolite facies) at Salobo than at the other systems (greenschist facies). The Cinzento strike-slip fault system—one of the more prominent regional structures associated with these deposits—was active at 2.5 Ga (Pinheiro & Holdsworth 1997), (Requia *et al.* 2003), Requia *et al.* (2003) interpret multiple Re-Os (molybdenite) mineralization ages at Salobo (2576 ± 6 and 2572 ± 8 Ma) to represent reactivation of the shear zone and brittle structures that control the orientation of the orebody.

From comparing the Fennoscandian shield and Carajàs districts to the Cloncurry District, a clear association can be made between ductile or ductile-brittle structural settings, and the formation of replacement IOCG orebodies such as the E1 Group, Nautanen and Salobo.

Multiple factors may explain the presence of both breccia-hosted and shear-hosted IOCG deposits in these regions. In the case of the Carajás District, the variation in deformation style between Salobo and other deposits may be attributable to the grade of metamorphism (Grainger *et al.* 2008), with Salobo forming in a higher-grade zone dominated by ductile strain. Another factor that may be important is the volume of fluids expelled from possible source magmas, as previously discussed for Ernest Henry and the E1 Group; more fluids can lead to higher fluid pressure, causing brecciation. However, the large size of the Salobo orebody (789 Mt at 0.96% Cu and 0.52 g/t Au; Souza & Vieira 2000) indicates that shear zone replacement by magmatic fluids can form large IOCG deposits. Instead, the rate of fluid flow is probably more important, with breccia orebodies possibly characterized by higher rates. Lastly, late brittle deformation and mineralization may take place in systems affected by earlier metasomatism. For example, Billström *et al.* (2010) suggested that earlier Na-Ca and/or magnetite/hematite alteration structurally prepared the host rocks of some deposits (e.g. Gruvberget-Cu?) in this district for hydrothermal brecciation by increasing their rigidity.

Regardless of structural regime, deposits in all three districts are commonly controlled by shifts in the competency of the host rocks. Examples of this are apparent at Salobo, where ores are hosted in a metagreywacke bounded by more competent quartzite and gneiss (Requia *et al.* 2003). In the Fennoscandian shield, deposits such as Nautanen and Aitik are hosted within schist surrounded by gneiss and granite (Billström *et al.* 2010). Overall, it is clear that the structural controls and setting of the E1 Group and Ernest Henry deposits are comparable to IOCGs in other provinces, and the results presented in this study may be applied to shear-hosted, replacement-style IOCG orebodies elsewhere.

Conclusions

Three-dimensional geological modeling and geochemical interpolation, when combined with drill core and open pit observations, can facilitate the spatial and temporal understanding of deposit evolution. The E1 Group of Fe-oxide Cu-Au deposits is characterized by four major deformational events recognizable at small scales through drill core logging, and at large scales through deposit-scale modeling. Although much of the mineralization in the E1 Group is hosted within metasedimentary rocks, the E1 North orebody is substantially larger than other orebodies in the Group due to the intersection of the E1 North Shear Zone with the Corella Marble horizon. Mineralization took place during local D₃ / regional D₄ shearing and

faulting in a transpressional Riedel brittle to ductile system associated with the major Cloncurry Fault Zone. At E1 North, this deformation was focused along the E1 North Shear Zone trending northeast and parallel with the west limb of the north-northwest plunging E1 North Antiform. Fluids at E1 South were focused in the hinge of the E1 South Synform. Ernest Henry mineralization also took place during local D₃ / regional D₄ and was focused in reverse sense shear zones.

Mineralization at the Ernest Henry breccia-hosted deposit was facilitated by strain partitioning between ductile metasedimentary or biotite-rich metavolcanic rocks, surrounding a more competent sequence of Mount Fort Constantine metavolcanic rocks which deformed through fracturing. In contrast, at the E1 Group replacement deposit, only one layer of metasedimentary rock was aligned to northeast-trending shear zones, causing strain and mineralization to focus mostly into the metasedimentary rock layer. Additionally, strain rate and fluid pressure may have been lower at the E1 Group than at Ernest Henry. The mineralizing fluids permeated through shear zones and chemically replaced metasedimentary rocks in the rest of the system.

Relative permeability and degree of fluid overpressure (where fluid pressure > lithostatic pressure) are important characteristics influencing the formation of Ernest Henry-style IOCG breccia orebodies, as opposed to shear-zone replacement-style E1 Group orebodies. These are in addition to factors such as magma fertility, and the degree of mixing between multiple potential source fluids. In the northeast Cloncurry District, northeast-trending structures intersecting folded metasedimentary horizons, and hosted within conjugate-trending strike-slip structures, can form shear systems ideal for Ernest Henry and E1 Group-styles of mineralization. In some instances, juxtaposition of competent lithologies, such as metavolcanic rocks, between multiple metasedimentary rock horizons facilitates the brecciation necessary to form Ernest Henry-sized IOCG systems. The E1 Group and Ernest Henry-style orebodies occur in other districts including the Fennoscandian shield and Carajás. Replacement bodies like the E1 Group tend to form in ductile-brittle or ductile regimes, whereas breccia ores are more commonly, but not exclusively, associated with more brittle regimes. Rheology contrasts in the country rocks are important for focusing the structures that control these types of IOCG deposits.

Acknowledgements

This paper forms a component of the first author's PhD dissertation at James Cook University. We would like to thank the following organizations for funding of this research: James Cook University, Mount Isa Mines and Ernest Henry Mining (subsidiaries of Glencore), the Society of Economic Geologists Foundation (Awards GSF 13-31 and SRG 14-93), the Economic Geology Research Centre (EGRU), and the Dr Schürmann Foundation (Grant 98/2014). Aranz Geo generously supplied an academic license for the use of Leapfrog. The paper was substantially improved through feedback from the reviewers J. Kolb and F. Bierlein, and from the editor K. Gessner.

References

- Abu Sharib, A.S. A. A. & Bell, T.H. 2011. Radical changes in bulk shortening directions during orogenesis: Significance for progressive development of regional folds and thrusts. *Precambrian Research*, **188**, 1–20.
- Adshead-Bell, N. 1998. Evolution of the Starra and Selwyn high-strain zones, Eastern fold belt, Mount Isa Inlier; implications for Au-Cu mineralization. *Economic Geology*, **93**, 1450–1462.
- Alcaraz, S., Lane, R. & Spragg, K. 2011. 3D geological modelling using new Leapfrog Geothermal software. *In: Proceedings, Thirty-Sixth Workshop on Geothermal Reservoir Engineering*, Stanford University, Stanford, California, USA, Jan 31 – Feb 2, 2011, SGP-TR-191. https://pangea.stanford.edu/ERE/db/IGAstandard/record_detail.php?id=7165.
- Austin, J. R. & Blenkinsop, T. G. 2010. Cloncurry Fault Zone: strain partitioning and reactivation in a crustal-scale deformation zone, Mt Isa Inlier. *Australian Journal of Earth Sciences*, **57**, 1–21.
- Austin, J. & Blenkinsop, T. 2008. The Cloncurry Lineament: Geophysical and geological evidence for a deep crustal structure in the Eastern Succession of the Mount Isa Inlier. *Precambrian Research*, **163**, 50–68.
- Baker, T. 1998. Alteration, mineralization, and fluid evolution at the Eloise Cu-Au deposit, Cloncurry District, northwest Queensland, Australia. *Economic Geology*, **93**, 1213–1236.

- Baker, T. & Laing, W. 1998. Eloise Cu-Au deposit, East Mt Isa Block: Structural environment and structural controls on ore. *Australian Journal of Earth Sciences*, **55**, 429–444.
- Barton, M.D., & Johnson, D.A. 2000. Alternative brine sources for Fe-oxide(-Cu-Au) systems: Implications for hydrothermal alteration and metals. In: Porter, T.M. (ed.) *Hydrothermal Iron Oxide Copper-Gold and Related Deposits: a Global Perspective*. **Vol. 1**. PGC Publishing, Adelaide, 123–136.
- Beardsmore, T.J. 1992. *Petrogenesis of Mount Dore-style breccia-hosted copper ± gold mineralization in the Kuridala-Selwyn region of northwestern Queensland*. Unpublished PhD thesis James Cook University, Queensland, Australia.
- Bell, T. 1983. Thrusting and duplex formation at Mount Isa, Queensland, Australia. *Nature*, **304**, 493–497.
- Bell, T.H. & Hickey, K.A. 1998. Multiple deformations with successive subvertical and subhorizontal axial planes in the Mount Isa region; their impact on geometric development and significance for mineralization and exploration. *Economic Geology*, **93**, 1369–1389.
- Billström, K, Eilu, P., Martinsson, O., Niiranen, T., Broman, C., Weihed, P., Wanhainen, C. & Ojala, J. 2010. IOCG and related mineral deposits of the Northern Fennoscandian Shield In: Porter, T. M. (ed.) *Hydrothermal Iron Oxide Copper-Gold and Related Deposits: A Global Perspective*, **4**, PGC Publishing, Adelaide, Australia, 381-414.
- Blake, D. H. 1987. *Geology of the Mount Isa Inlier and environs, Queensland and Northern Territory* (Vol. 225). Australian Government Public Service.
- Blake, D. H. & Stewart, A. J. 1992. Stratigraphic and tectonic framework, Mount Isa Inlier. In: Stewart, A. J., Blake, D. H. (eds) *Detailed Studies of the Mount Isa Inlier*. Australian Geological Survey Organization, Bulletin 243, 1–12.
- Blenkinsop, T., Huddleston-Holmes, C., et al. 2008. The crustal scale architecture of the Eastern Succession, Mount Isa: The influence of inversion. *Precambrian Research*, **163**, 31–49.

- Belperio, A., Flint, R. & Freeman, H. 2007. Prominent Hill: A Hematite-Dominated, Iron Oxide Copper-Gold System. *Economic Geology*, **102**, 1499–1510.
- Betts, P. & Giles, D. 2006. The 1800–1100Ma tectonic evolution of Australia. *Precambrian Research*, **144**, 92–125.
- Cloos, H. 1928. Experimenten zur inneren Tektonik. *Centralblatt fur Mineralogie and Paleontologie*, **1928B**, 609.
- Cowan, E., Beatson, R., Ross, H., Fright, W., McLennan, T., Evans, T. & Titley, M. 2003. Practical implicit geological modelling. In: *Fifth International Mining Geology Conference Proceedings*, Bendigo, Victoria, Australia, Nov 17-19 2003, 89–99.
<https://www.ausimm.com.au/publications/publication.aspx?ID=188>
- Coward, M. 2001. *Structural Controls on Ore Formation and Distribution at the Ernest Henry Cu-Au Deposit, NW Qld*. Unpublished Honours Thesis, James Cook University.
- Davidson, G. J., Davis, B. K. & Garner, A. 2002. Structural and geochemical constraints on the emplacement of the Monakoff oxide Cu-Au (-Co-U-REE-Ag-Zn-Pb) deposit, Mt Isa Inlier, Australia. In: Porter, T. M. (ed.) *Hydrothermal Iron Oxide Copper-Gold and Related Deposits: A Global Perspective*, **2**, PGC Publishing, Adelaide, Australia, 49–75.
- Davis, G. H., Bump, A. P., Garcia, P. E. & Ahlgren, S. G. 2000. Conjugate Riedel deformation band shear zones. *Journal of Structural Geology*, **22**, 169–190.
- Duncan, R., Stein, H., Evans, K., Hitzman, M. W., Nelson, E. & Kirwin, D. 2011. Geochronological Framework for Mineralization and Alteration in the Selwyn-Mount Dore Corridor, Eastern Fold Belt, Mount Isa Inlier, Australia: Genetic Implications. *Economic Geology*, **106**, 169–192.
- Duncan, R. J., Hitzman, M. W., Nelson, E. P. & Togtokhbayar, O. 2014. Structural and lithological controls on iron oxide copper-gold deposits of the Southern Selwyn-Mount Dore Corridor, Eastern Fold Belt, Queensland, Australia. *Economic Geology*, **109**, 419–456.
- Fisher, L. & Kendrick, M. 2008. Metamorphic fluid origins in the Osborne Fe oxide-Cu-Au deposit, Australia: evidence from noble gases and halogens. *Mineralium Deposita*, **43**, 483–497.

Foster, D. R. W. & Austin, J. 2008. The 1800–1610 Ma stratigraphic and magmatic history of the Eastern Succession, Mount Isa Inlier, and correlations with adjacent Paleoproterozoic terranes. *Precambrian Research*, **163**, 7–30.

Foster, D. R. W. & Rubenach, M. J. 2006. Isograd pattern and regional low-pressure, high-temperature metamorphism of pelitic, mafic and calc-silicate rocks along an east-west section through the Mt Isa Inlier. *Australian Journal of Earth Sciences*, **53**, 167–186.

Gauthier, L., Hall, G., Stein, H. & Schaltegger, U. 2001. The Osborne deposit, Cloncurry district: a 1595 Ma Cu-Au skarn deposit. In: Williams P. J. (ed.) *A Hydrothermal Odyssey*. Extended Conference Abstracts. Contributions of the Economic Geology Research Unit 59, James Cook University, Townsville, Australia, 58–59.

Geological Survey of Queensland. 2011. *Northwest Queensland Minerals and Energy Province Report*. Queensland Department of Employment, Economic Development and Innovation, Brisbane, 102p.

Gessner, K., Jones, P.A., Wilde, A.R. & Kühn, M. 2006. Significance of strain localization and fracturing in relation to hydrothermal mineralization at Mount Isa, Australia. *Journal of Geochemical Exploration*, **89**, 129–132.

Gessner, K. 2009. Coupled models of brittle-plastic deformation and fluid flow: Approaches, methods, and application to mesoproterozoic mineralisation at mount Isa, Australia. *Surveys in Geophysics*, **30**, 211–232.

Giles, D. & Nutman, A. 2002. SHRIMP U-Pb monazite dating of 1600–1580 Ma amphibolite facies metamorphism in the southeastern Mt Isa Block, Australia. *Australian Journal of Earth Sciences*, **49**, 455–465.

Giles, D., Betts, P.G., Aillères, L., Hulscher, B., Hough, M. & Lister, G.S. 2006. Evolution of the Isan Orogeny at the southeastern margin of the Mt Isa Inlier. *Australian Journal of Earth Sciences*, **53**, 91–108.

Grainger, C.J., Groves, D.I., Tallarico, F.H.B. & Fletcher, I.R. 2008. Metallogenesis of the Carajás Mineral Province, Southern Amazon Craton, Brazil: Varying styles of Archean

through Paleoproterozoic to Neoproterozoic base- and precious-metal mineralisation. *Ore Geology Reviews*, **33**, 451–489.

Groves, D. I., Bierlein, F. P., Meinert, L. D. & Hitzman, M. W. 2010. Iron oxide copper–gold (IOCG) deposits through Earth history: Implications for origin, lithospheric setting, and distinction from other epigenetic iron oxide deposits. *Economic Geology*, **105**, 641–654.

Haynes, D. W. 2000. Iron oxide copper (-gold) deposits: Their position in the ore deposit spectrum and modes of origin. In: Porter, T. M. (ed.) *Hydrothermal Iron Oxide Copper-Gold and Related Deposits: A Global Perspective, I*, PGC Publishing, Adelaide, Australia, 71-90.

Haynes, D.W., Cross, K.C., Bills, R.T. & Reed, M.H. 1995. Olympic Dam ore genesis: a fluid-mixing model. *Economic Geology*, **90**, 281–307.

Hill, E. J., Oliver, N. H. S., Cleverley, J. S., Nugus, M. J., Carswell, J. & Clark, F. 2014. Characterisation and 3D modelling of a nuggety, vein-hosted gold ore body, Sunrise Dam, Western Australia. *Journal of Structural Geology*, **67**, 222–234.

Hitzman, M. W., Oreskes, N. & Einaudi, M.T. 1992. Geological characteristics and tectonic setting of proterozoic iron oxide (Cu-U-Au-REE) deposits. *Precambrian Research*, **58**, 241–287.

Hitzman, M. W. 2000. Iron oxide-Cu-Au deposits: What, where, when and why. In: Porter, T. M. (ed.) *Hydrothermal Iron Oxide Copper-Gold and Related Deposits: A Global Perspective, I*, PGC Publishing, Adelaide, Australia, 9–25.

Hunt, J., Baker, T. & Thorkelson, D. 2007. A review of iron oxide copper-gold deposits, with focus on the Wernecke Breccias, Yukon, Canada, as an example of a non-magmatic end member and implications for IOCG genesis and classification. *Exploration and Mining Geology*, **16**, 209–232.

Kamb, W.B. 1959. Ice petrofabric observations from Blue Glacier, Washington, in relation to theory and experiment. *Journal of Geophysical Research*, **64**, 1891–1909.

Kendrick, M. A., Mark, G. & Phillips, D. 2007. Mid-crustal fluid mixing in a Proterozoic Fe oxide–Cu–Au deposit, Ernest Henry, Australia: Evidence from Ar, Kr, Xe, Cl, Br, and I. *Earth and Planetary Science Letters*, **256**, 328–343.

- Kirchenbaur, M., Maas, R., Ehrig, K., Kamenetsky, V.S., Strub, E., Ballhaus, C. & Münker, C. 2016. Uranium and Sm isotope studies of the supergiant Olympic Dam Cu-Au-U-Ag deposit, South Australia. *Geochimica et Cosmochimica Acta*, **180**, 15–32.
- Loosveld, R. & Schreurs, G. 1987. Discovery of thrust klippen, northwest of Mary Kathleen, Mt Isa Inlier, Australia. *Australian Journal of Earth Sciences*, **34**, 387–402.
- Macmillan, E., Cook, N.J., Ehrig, K., Ciobanu, C.L. & Pring, A. 2016. Uraninite from the Olympic Dam IOCG-U-Ag deposit : linking textural and compositional variation to temporal evolution. *American Mineralogist*, **101**, 1295–1320.
- Mark, G.M., Stein, H. & Salt, C. 2004. Re-Os isotopic evidence for two periods of sulfide mineralisation in the vicinity of the Ernest Henry Cu-Au deposit, northwest Queensland, Australia. *In: AGC Geological Society of Australia: Proceedings, 17th*. 96.
- Mark, G., Oliver, N.H.S., Williams, P.J., Valenta, R.K. & Crookes, R.A., 2000. The evolution of the Ernest Henry Fe-Oxide-(Cu-Au) hydrothermal system. *In: Porter, T. M. (ed.) Hydrothermal Iron Oxide Copper-Gold and Related Deposits: A Global Perspective, 1*, PGC Publishing, Adelaide, Australia, 123–136.
- Mark, G., Oliver, N.H.S. & Williams, P.J. 2006. Mineralogical and chemical evolution of the Ernest Henry Fe oxide–Cu–Au ore system, Cloncurry district, northwest Queensland, Australia. *Mineralium Deposita*, **40**, 769–801.
- Marschik, R. & Fontboté, L. 2001. The Candelaria-Punta del Cobre iron oxide Cu-Au (-Zn-Ag) deposits, Chile. *Economic Geology*, **96**, 1799–1826.
- Marshall, L. & Oliver, N. 2008. Constraints on hydrothermal fluid pathways within Mary Kathleen Group stratigraphy of the Cloncurry iron-oxide–copper–gold District, Australia. *Precambrian Research*, **163**, 151–158.
- Martinsson, O. & Wanhainen, C. 2004. Character of Cu-Au mineralization and related hydrothermal alterations along the Nautanen deformation zone, Gällivare area, northern Sweden. *In: Allen, R., Martinsson, O. and Weihed, P., (eds.), Svecofennian Ore-Forming Environments Field Trip: Volcanic-associated Zn-Cu-Au-Ag and Magnetite-apatite, Sedimen-*

hosted Pb-Zn, and Intrusion-associated Cu-Au Deposits in Northern Sweden. Society of Economic Geologists Guidebook Series, **33**, 149-160.

McLellan, J.G., Mustard, R., Blenkinsop, T., Oliver, N. H. S., & McKeagney, C. 2010. Critical ingredients of IOCG mineralisation in the Eastern Fold Belt of the Mount Isa Inlier: Insights from combining spatial analysis with mechanical numerical modeling. *In: Porter, T. M. (ed.) Hydrothermal Iron Oxide Copper-Gold and Related Deposits: A Global Perspective*, **3**, PGC Publishing, Adelaide, Australia, 233-256.

Meinert, L.D. 1992. Skarns and skarn deposits. *Geoscience Canada*, **19**, 145–162.

Murphy, F.C., Hutton, L.J., et al. 2011. Mineral system analysis of the Mt Isa-McArthur River region, Northern Australia. *Australian Journal of Earth Sciences*, **58**, 849–873.

Neumann, N.L., Southgate, P.N., Gibson, G.M. & MCintyre, a. 2006. New SHRIMP geochronology for the Western Fold Belt of the Mt Isa Inlier: developing a 1800 – 1650 Ma event framework. *Australian Journal of Earth Sciences*, **53**, 1023–1039.

O’Dea, M. G., Lister, G. S., Maccready, T., Betts, P. G., Oliver, N. H. S., Pound, K. S. & Valenta, R. K. 1997. Geodynamic evolution of the Proterozoic Mount Isa terrain. *Geological Society, London, Special Publications*, **121**, 99–122.

O’Dea, M. G., Betts, P. G., MacCready, T. & Aillères, L. 2006. Sequential development of a mid-crustal fold-thrust complex: evidence from the Mitakoodi Culmination in the eastern Mt Isa Inlier, Australia. *Australian Journal of Earth Sciences*, **53**, 69–90.

Oliver, N.H.S., Cleverley, J.S., et al. 2004. Modeling the role of sodic alteration in the genesis of iron oxide-copper-gold deposits, eastern Mount Isa block, Australia. *Economic Geology*, **99**, 1145–1176.

Oliver, N.H.S., Rubenach, M.J., et al. 2006. Granite-related overpressure and volatile release in the mid crust: fluidized breccias from the Cloncurry District, Australia. *Geofluids*, **6**, 346–358.

- Oliver, N., Butera, K., Rubenach, M., Marshall, L., Cleverley, J., Mark, G., Tullemans, F. & Esser, D. 2008. The protracted hydrothermal evolution of the Mount Isa Eastern Succession: A review and tectonic implications. *Precambrian Research*, **163**, 108–130.
- Oreskes, N. & Einaudi, M. 1990. Origin of rare earth element-enriched hematite breccias at the Olympic Dam Cu-U-Au-Ag deposit, Roxby Downs, South Australia. *Economic Geology*, **85**, 1–28.
- Oreskes, N. & Einaudi, M.T. 1992. Origin of hydrothermal fluids at Olympic Dam; preliminary results from fluid inclusions and stable isotopes. *Economic Geology*, **87**, 64–90.
- Page, R. W. & Sun, S. 1998. Aspects of geochronology and crustal evolution in the Eastern Fold Belt, Mt Isa Inlier. *Australian Journal of Earth Sciences*, **45**, 343–361.
- Page, R.W. & Williams, I.S. 1988. Age of the barramundi orogeny in northern Australia by means of ion microprobe and conventional U-Pb zircon studies. *Precambrian Research*, **40-41**, 21–36.
- Pinheiro, R.V.L. & Holdsworth, R.E. 1997. Reactivation of Archaean strike-slip fault systems, Amazon region, Brazil. *Journal of the Geological Society*, **154**, 99–103.
- Pollard, P. J. 2000. Evidence of a magmatic fluid and metal source for Fe-oxide Cu-Au mineralization. In: Porter, T. M. (ed.) *Hydrothermal Iron Oxide Copper-Gold and Related Deposits: A Global Perspectiv. I*, PGC Publishing, Adelaide, Australia, 27–41.
- Reimann, C. 2005. Geochemical mapping: technique or art? *Geochemistry: Exploration, Environment, Analysis*, **5**, 359–370.
- Requia, K., Stein, H., Fontbote, L. & Chiaradia, M. 2003. Re-Os and Pb-Pb geochronology of the Archean Salobo iron oxide copper-gold deposit, Carajas mineral province, northern Brazil. *Mineralium Deposita*, **38**, 727–738.
- Riedel, W. 1929. Zur Mechanik geologischer Brucherscheinungen. *Zentralblatt für Minerologie, Geologie, und Paleontologie* **1929B**, 354.

Ronzê, P.C., Soares, A.D.V., Santos, M.G.S & Barreira, C.F. 2000. Alemão copper-gold (U-REE) deposit, Carajás, Brazil. *In: Porter, T. M. (ed.) Hydrothermal Iron Oxide Copper-Gold and Related Deposits: A Global Perspective, I*, PGC Publishing, Adelaide, Australia, 191-202.

Rubenach, M. & Barker, A. 1998. Metamorphic and metasomatic evolution of the Snake Creek Anticline, Eastern Succession, Mt Isa Inlier. *Australian Journal of Earth Sciences*, **45**, 37–41.

Rubenach, M. & Lewthwaite, K. 2002. Metasomatic albitites and related biotite-rich schists from a low-pressure polymetamorphic terrane, Snake Creek Anticline, Mount Isa Inlier, north-eastern Australia: microstructures and P-T-d paths. *Journal of Metamorphic Geology*, **20**, 191–202.

Rubenach, M., Foster, D., Evins, P., Blake, K. & Fanning, C. 2008. Age constraints on the tectonothermal evolution of the Selwyn Zone, Eastern Fold Belt, Mount Isa Inlier. *Precambrian Research*, **163**, 81–107.

Rusk, B.G., Oliver, N.H.S., Cleverly, J.S., Blenkinsop, T.G., Zhang, D., Williams, P.J. & Habermann, P. 2010. Physical and chemical characteristics of the Ernest Henry iron oxide copper gold deposit, Australia: Implications for IOCG genesis. *In: Porter, T.M. (ed.), Hydrothermal Iron Oxide Copper-Gold and Related Deposits: A Global Perspective, 4*, PGC Publishing, Adelaide, Australia, 201-218.

Stewart, M., de Lacey, J., Hodkiewicz, P.F. & Lane, R. 2014. Grade Estimation from Radial Basis Functions – How Does it Compare with Conventional Geostatistical Estimation? *In: Ninth International Mining Geology Conference*. Adelaide, Australia, 129–139.

Souza, L. H. & Vieira, E. A. P. 2000. Salobo Alpha 3 deposit: Geology and mineralisation. *In: Porter, T. M. (ed.) Hydrothermal Iron Oxide Copper-Gold and Related Deposits: A Global Perspective, I*, PGC Publishing, Adelaide, Australia, 213-224.

Tukey, J. W. 1977. *Exploratory Data Analysis*. Addison-Wesley, Reading.

Twyerould, S. C. 1997. *The geology and genesis of the Ernest Henry Fe–Cu–Au deposit, northwest Queensland, Australia*. Unpublished PhD thesis, Eugene, Oregon, University of Oregon, USA.

Vine, J. D., and Tourtelot, E.B. 1970. Geochemistry of black shale deposits; a summary report. *Economic Geology* **65**: 253-272.

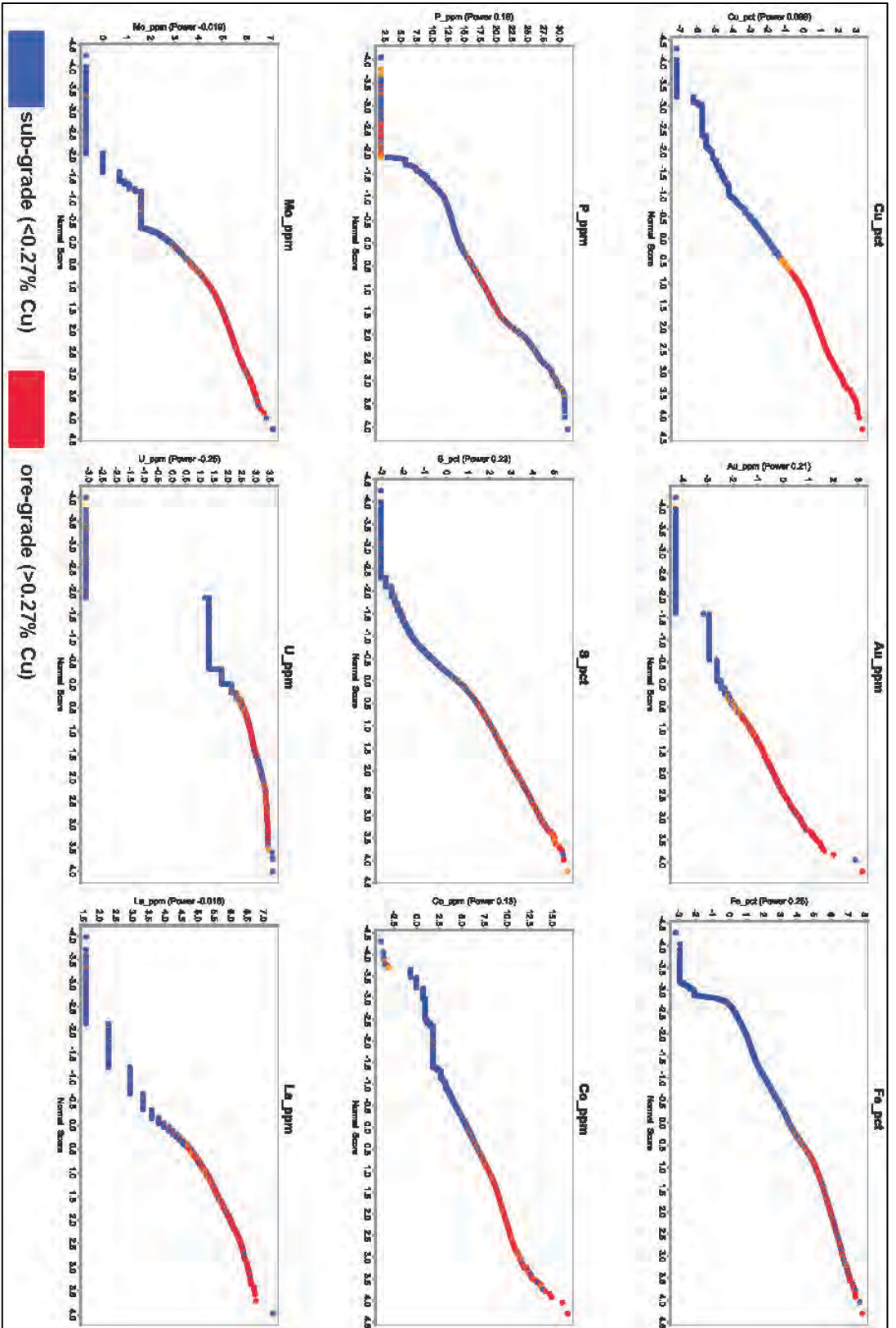
Wang, S. & Williams, P. J. 2001. Geochemistry and origin of Proterozoic skarns at the Mount Elliott Cu-Au(-Co-Ni) deposit, Cloncurry district, NW Queensland, Australia. *Mineralium Deposita*, **36**, 109–124.

Williams, P., Barton, M., et al. 2005. Iron Oxide Copper-Gold Deposits: Geology, Space-Time Distribution, and Possible Modes of Origin. In: Hedenquist, J. W., Thompson, J. F. H., Goldfarb, R. J. & Richards, J. P. (eds), *Economic Geology 100th Anniversary Volume*, Society of Economic Geologists, Inc.

Williams, M. R., Holwell, D. A., Lilly, R. M., Case, G. N. D. & McDonald, I. 2015. Mineralogical and fluid characteristics of the fluorite-rich Monakoff and E1 Cu-Au deposits, Cloncurry region, Queensland, Australia: implications for regional F-Ba-rich IOCG mineralization. *Ore Geology Reviews*, **64**, 103-127.

Wyborn, L. & Page, R. 1983. The Proterozoic Kalkadoon and Ewen Batholiths, Mount Isa Inlier, Queensland: source, chemistry, age and metamorphism. *BMR Journal of Australian Geology & Geophysics*, **8**, 53–69.

Wyborn, L., Page, R. & McCulloch, M. 1988. Petrology, geochronology and isotope geochemistry of the post-1820 Ma granites of the Mount Isa Inlier: mechanisms for the generation of Proterozoic anorogenic granites. *Precambrian Research*, **40-41**, 509–541.



Appendix 1: Probability plots of assay data for modelled elements. Plots made in ioGAS software. Power transform applied to y-axes of all elements. Note that Fe, P, and S do not follow normal / log-normal distributions.

Appendix 2: Summary Statistics for Interpolated Elements									
	Cu	Au	Fe	P	S	Co	Mo	U	La
Count Numeric	58723	38933	56200	20017	45976	57026	48781	16350	14031
Count Text	0	0	0	0	0	0	0	0	0
Count Null	0	19790	2523	38706	12747	1697	9942	42373	44692
Count Negative	0	0	0	0	0	0	0	0	0
Count Zero	39	2125	0	0	0	0	0	0	0
Unique Values	2569	218	4317	2004	1793	962	556	786	109
Minimum	0	0	0	5	0	0	1	0	5
Maximum	19	11	77	26600	36	7600	2037	6786	2260
Mean	0	0	15	1682	3	124	50	79	120
Median	0	0	13	980	2	69	18	19	60
Standard Deviation	1	0	10	2185	3	160	77	204	143
Interquartile Range	0	0	15	1370	4	140	59	65	150
Range	19	11	77	26595	36	7600	2037	6786	2255
1 percentile	0	0	2	5	0	5	1	0	5
5 percentile	0	0	3	100	0	5	1	5	10
10 percentile	0	0	4	280	0	10	3	5	10
25 percentile	0	0	7	630	0	24	5	5	20
75 percentile	0	0	22	2000	4	164	64	70	170
90 percentile	1	0	30	3430	7	326	149	160	300
95 percentile	2	0	34	4750	8	428	203	320	400
99 percentile	3	1	42	11950	13	669	336	1162	680